24. Maruyama T, Kanaji T, Nakade S, Kanno T, Mikoshiba K (1997) 2APB, 2-aminoethoxydiphenyl borate, a membrane-penetrable modulator of Ins(1,4,5)P3-induced Ca2+ release. J Biochem 122: 498–505.
25. O'Keefe SJ, Tamura J, Kincaid RL, Tocci MJ, O'Neill EA (1992) FK-506- and CsA-sensitive activation of the interleukin-2 promoter by calcineurin. Nature 357: 692–694.
26. Saneyoshi T, Kume S, Amasaki Y, Mikoshiba K (2002) The Wnt/calcium pathway activates NF-AT and promotes ventral cell fate in Xenopus embryos. Nature 417: 295–299.
27. Jayaraman T, Marks AR (2000) Calcineurin is downstream of the inositol 1,4,5-trisphosphate receptor in the apoptotic and cell growth pathways. J Biol Chem 275: 6417–6420.
28. Johnson EN, Lee YM, Sander TL, Rabkin E, Schoen FJ, et al. (2003) NFATc1 mediates vascular endothelial growth factor-induced proliferation of human pulmonary valve endothelial cells. J Biol Chem 278: 1686–1692.
29. Brock TA, Dvorak HF, Senger DR (1991) Tumor-secreted vascular permeability factor increases cytosolic Ca2+ and von Willebrand factor release in human endothelial cells. Am J Pathol 138: 213–221.
30. Zhou B, Cron RQ, Wu B, Genin A, Wang Z, et al. (2002) Regulation of the murine Nfatc1 gene by NFATc2. J Biol Chem 277: 10704–10711.
31. Oka T, Dai YS, Molkentin JD (2005) Regulation of calcineurin through transcriptional induction of the calcineurin A beta promoter in vitro and in vivo. Mol Cell Biol 25: 6649–6659.
32. Graef IA, Mermelstein PG, Stankunas K, Neilson JR, Deisseroth K, et al. (1999) L-type calcium channels and GSK-3 regulate the activity of NF-ATc4 in hippocampal neurons. Nature 401: 703–708.
33. Bootman MD, Collins TJ, Mackenzie L, Roderick HL, Berridge MJ, et al. (2002) 2-aminoethoxydiphenyl borate (2-APB) is a reliable blocker of store-operated Ca2+ entry but an inconsistent inhibitor of InsP3-induced Ca2+ release. Faseb J 16: 1145–1150.
34. Arron JR, Winslow MM, Polleri A, Chang CP, Wu H, et al. (2006) NFAT dysregulation by increased dosage of DSCR1 and DYRK1A on chromosome 21. Nature 441: 595–600.
35. Maeda N, Niinobe M, Nakahira K, Mikoshiba K (1988) Purification and characterization of P400 protein, a glycoprotein characteristic of Purkinje cell, from mouse cerebellum. J Neurochem 51: 1724–1730.
36. Sugiyama T, Furuya A, Monkawa T, Yamamoto-Hino M, Satoh S, et al. (1994) Monoclonal antibodies distinctively recognizing the subtypes of inositol 1,4,5-trisphosphate receptor: application to the studies on inflammatory cells. FEBS Lett 354: 149–154.
37. Yamagishi H, Olson EN, Srivastava D (2000) The basic helix-loop-helix transcription factor, dHAND, is required for vascular development. J Clin Invest 105: 261–270.

Journal of Molecular and Cellular Cardiology 49 (2010) 576–586

Contents lists available at ScienceDirect

Journal of Molecular and Cellular Cardiology

journal homepage: www.elsevier.com/locate/yjmcc

Original article

4-Hydroxy-2-nonenal protects against cardiac ischemia–reperfusion injury *via* the Nrf2-dependent pathway

Yan Zhang [a,1], Motoaki Sano [a,d,*], Ken Shinmura [b], Kayoko Tamaki [b], Yoshinori Katsumata [a], Tomohiro Matsuhashi [a], Shintaro Morizane [a], Hideyuki Ito [a], Takako Hishiki [c], Jin Endo [a], Heping Zhou [a], Shinsuke Yuasa [a], Ruri Kaneda [a], Makoto Suematsu [c], Keiichi Fukuda [a]

[a] Department of Cardiology, Keio University School of Medicine, Tokyo, 160-8582, Japan
[b] Department of Geriatric Medicine, Keio University School of Medicine, Tokyo, 160-8582, Japan
[c] Department of Biochemistry and Integrative Medical Biology, Keio University School of Medicine, Tokyo, 160-8582, Japan
[d] Precursory Research for Embryonic Science and Technology (PRESTO), Japan Science and Technology Agency, Saitama, 332-0012, Japan

ARTICLE INFO

Article history:
Received 25 December 2009
Received in revised form 24 April 2010
Accepted 21 May 2010
Available online 4 June 2010

Keywords:
4-Hydroxy-2-nonenal
Ischemia–reperfusion injury
Nrf2
Hormesis
Glutathione

ABSTRACT

Reactive oxygen species (ROS) attack polyunsaturated fatty acids of the membrane and trigger lipid peroxidation, which results in the generation of α,β-unsaturated aldehydes, such as 4-hydroxy-2-nonenal (4-HNE). There is compelling evidence that high concentrations of aldehydes are responsible for much of the damage elicited by cardiac ischemia–reperfusion injury, while sublethal concentrations of aldehydes stimulate stress resistance pathways, to achieve cardioprotection. We investigated the mechanism of cardioprotection mediated by 4-HNE. For cultured cardiomyocytes, 4-HNE was cytotoxic at higher concentrations (≥20 μM) but had no appreciable cytotoxicity at lower concentrations. Notably, a sublethal concentration (5 μM) of 4-HNE primed cardiomyocytes to become resistant to cytotoxic concentrations of 4-HNE. 4-HNE induced nuclear translocation of transcription factor NF-E2-related factor 2 (Nrf2), and enhanced the expression of γ-glutamylcysteine ligase (GCL) and the core subunit of the Xc^- high-affinity cystine transporter (xCT), thereby increasing 1.45-fold the intracellular GSH levels. Cardiomyocytes treated with either Nrf2-specific siRNA or the GCL inhibitor L-buthionine sulfoximine (BSO) were less tolerant to 4-HNE. Moreover, the cardioprotective effect of 4-HNE pretreatment against subsequent glucose-free anoxia followed by reoxygenation was completely abolished in these cells. Intravenous administration of 4-HNE (4 mg/kg) activated Nrf2 in the heart and increased the intramyocardial GSH content, and consequently improved the functional recovery of the left ventricle following ischemia–reperfusion in Langendorff-perfused hearts. This cardioprotective effect of 4-HNE was not observed for Nrf2-knockout mice. In summary, 4-HNE activates Nrf2-mediated gene expression and stimulates GSH biosynthesis, thereby conferring on cardiomyocytes protection against ischemia–reperfusion injury.

1. Introduction

Reactive oxygen species (ROS) originate from various sources, including the Nox family of NADPH oxidases, xanthine oxidase, and mitochondria, in which superoxide radicals are the byproducts of oxidative energy production. Superoxide radicals are dismuted by superoxide dismutase (SOD), to produce hydrogen peroxides, which in turn are degraded into water and molecular oxygen by catalase, glutathione peroxidase (Gpx), and peroxiredoxin (Prx). Hydroxyl radicals (OH•), which are the most potent ROS, are formed from hydrogen peroxides through the Fenton reaction. No endogenous enzymes exist to eliminate these radicals. The OH• attack neighboring polyunsaturated fatty acids in the cell membrane, thereby triggering lipid peroxidation, which results in the generation of lipid hydroperoxides and α,β-unsaturated aldehydes, including 4-hydroxy-2-nonenal (4-HNE). These aldehydes are highly electrophilic and react with biomolecules, such as proteins and nucleic acids, to generate various adducts [1]. By virtue of their high chemical stability, these lipid peroxidation products diffuse greater distances than their precursor ROS, so they can disseminate oxidative injury and amplify damage. Aldehydes accumulation is found in ischemic, hypertrophic, and failing hearts, as well as in the oxidation of LDL [2], atherosclerotic lesions, and the brains of patients with Alzheimer's disease [3], and therefore, have been implicated in the pathogenesis of oxidative stress-associated diseases. Pretreatment with a small molecule activator of an aldehyde-detoxifying enzyme, aldehyde dehydrogenase 2

* Corresponding author. Department of Cardiology, Keio University School of Medicine, 35 Shinanomachi Shinjuku-ku, Tokyo, 160-8582, Japan. Tel.: +81 3 5363 3874; fax: +81 3 5363 3875.
E-mail address: msano@sc.itc.keio.ac.jp (M. Sano).
[1] Present address: Department of Pharmacology, Harbin Medical University, Harbin, China.

0022-2828/$ - see front matter © 2010 Elsevier Ltd. All rights reserved.
doi:10.1016/j.yjmcc.2010.05.011

(ALDH2), reduced infarct size by 60% in a rat model of ischemia–reperfusion injury [4], which indicates that much of the damage inflicted by ischemia–reperfusion is attributable to aldehydes generated in the ischemic heart.

Although the pathogenic effects of ROS are well established, antioxidant supplements for the prevention of cardiovascular events have been found to lack efficacy, and may even be harmful [5]. This discrepancy may be attributable to the dual role of ROS. ROS are not simply toxic byproducts, since they also play important roles in establishing antioxidant defense mechanisms. The sensing of aldehyde accumulation in injured tissues enables the cell to activate a variety of stress resistance pathways in a cell-type-specific manner, so as to counteract oxidative stress-mediated injury [6–8]. This induction of protective mechanisms by stressors is referred to as "stress-response hormesis" [9]. Therefore, aldehydes may be regarded as second messengers that propagate ROS-initiating favorable signaling.

In the present study, we investigated whether 4-HNE, which is one of the most abundant aldehydes produced by lipid peroxidation *in vivo*, induces stress-response hormesis in cultured cardiomyocytes and in *in vivo* hearts, and determined the underlying mechanisms.

2. Materials and methods

2.1. Animals

All animal experiments were reviewed and approved by the Institutional Animal Care and Use Committee at Keio University School of Medicine. Male C57BL/6 J mice at 10 weeks of age were obtained from CLEA Japan (Tokyo, Japan). Nrf2-knockout mice on a C57BL/6 J background were generated as previously described [10]. For comparison, Nrf2-wildtype mice (C57BL/6 J) were obtained from siblings of the Nrf2-knockout.

2.2. Cell culturing

Neonatal ventricular myocytes from 1- to 2-day-old Sprague–Dawley rats were subjected to Percoll gradient centrifugation and differential plating, to enrich for cardiac myocytes and to deplete non-myocytes [11]. Cell viability was determined using the LIVE/DEAD Viability/Cytotoxicity Assay Kit (Molecular Probes), which is based on the simultaneous determination of live and dead cells with the calcein AM and ethidium homodimer-1 probes, which are specific for intracellular esterase activity and membrane integrity, respectively. Fluorescence imaging of the cells (live cells were labeled green, whereas the nuclei of dead cells were labeled red) was performed with a fluorescence microscope (BZ-9000; Keyence).

2.3. Western blotting

Nuclear extracts were prepared as described previously [11]. The following rabbit polyclonal antibodies were used: anti-Nrf2 and anti-xCT (core subunit of the Xc^- high-affinity cystine transporter) (Santa Cruz Biotechnology); anti-HO1 (hemoxygenase-1), (Stressgen); anti-catalase and anti-Gclc (catalytic subunit of γ-glutamylcysteine ligase) (Abcam); anti-Gsta2 (glutathione-S-transferase A2) (Novus Biologicals); anti-4-HNE adduct (Calbiochem). Immunoreactive proteins were visualized using horseradish peroxidase-conjugated secondary antibodies, enhanced chemiluminescence (Amersham Biosciences), and the LAS-3000 luminoimager (Fujifilm).

2.4. Quantitative Real-Time PCR

Total RNA samples from cultured cardiomyocytes and hearts were prepared using the Trizol reagent (Invitrogen), according to manufacturer's instructions. Samples of total RNA (2 μg) were reverse-transcribed using the RNA PCR Kit (Takara Biotechnology, Japan), and the resulting cDNA was used as a PCR template. The mRNA levels were determined by Real-Time PCR with the ABI PRISM 7700 Sequence Detector (Applied Biosystems), according to the manufacturer's instructions. Predesigned gene-specific primer and probe sets (TaqMan Gene Expression Assays) were used. The 18s ribosomal RNA was amplified as an internal control. The relative gene expression level (the amount of target, normalized to the endogenous control gene) was calculated using the comparative Ct method formula: $2^{-\Delta\Delta Ct}$.

2.5. siRNA oligonucleotides and transfection

The siRNA oligonucleotides directed against the rat Nrf2 and a control siRNA (Ambion) were transfected into cells using the Lipofectamine RNAiMAX reagent (Invitrogen) .

2.6. Determination of intracellular glutathione concentration

The intracellular concentration of GSH was measured spectrophotometrically (U-2810 spectrophotometer; Hitachi) using the Bioxytech GSH/GSSG-412 kit (Oxis Research), according to the manufacturer's instructions. All assays were performed in triplicate on at least three separate occasions.

2.7. Langendorff perfusion of the heart

Hearts were excised rapidly from heparinized mice, perfused with modified Krebs–Henseleit buffer (120 mmol/L NaCl, 25 mmol/L $NaHCO_3$, 5.9 mmol/L KCl, 1.2 mmol/L $MgSO_4$, 1.75 mmol/L $CaCl_2$, and 10 mmol/L glucose), and gassed with 95% O_2 and 5% CO_2 at 37 °C according to the Langendorff procedure. Coronary perfusion pressure was maintained at 90 mm Hg. A plastic catheter with a polyethylene balloon was inserted into the left ventricle (LV) through the left atrium. Before the induction of ischemia, the left ventricular end-diastolic pressure was adjusted to 10 mm Hg by filling the balloon with water. The indices of LV function, including LV systolic pressure (LVSP), LV end-diastolic pressure (LVEDP), and positive dP/dt, were recorded as described previously. The total lactate dehydrogenase (LDH) activity released into the perfusate was measured with a commercially available kit (Sigma) [11]. To examine the effect of 4-HNE treatment on function recovery after ischemia–reperfusion, mice were injected with either 4 mg/kg 4-HNE or vehicle (50 μl of saline) *via* the retro-orbital vein [12] [13]. The efficacy of injection via the retro-orbital vein was confirmed using Evans Blue (Supplemental Fig. 1).

2.8. Statistical analysis

The values are presented as mean ± SEM. Statistical significance was evaluated using 2-tailed, unpaired Student's *t*-tests for comparisons of two mean values. Multiple comparisons involving more than three groups were performed using ANOVA. A *P*-value less than 0.05 was considered statistically significant.

3. Results

3.1. High-dosage 4-HNE causes cardiomyocyte cell death

Neonatal rat cardiomyocytes were treated with various concentrations of 4-HNE for 24 h, and 4-HNE-induced cardiomyocyte toxicity was monitored (Fig. 1A, B). The viabilities of the cardiomyocytes in the presence of 0, 5, 10, 20, and 40 μM 4-HNE were 82.17% ± 3.19%, 80.96% ± 2.76%, 72.85% ± 2.06%, 28.95% ± 3.54%, and 0.00%, respectively (Fig. 1A). At concentrations >20 μM, HNE significantly decreased cell viability, whereas 5 μM or 10 μM 4-HNE showed no appreciable cytotoxicity. Based on these observations, concentrations of 4-HNE < 10 μM were selected for subsequent studies on the potential favorable effects of 4-HNE.

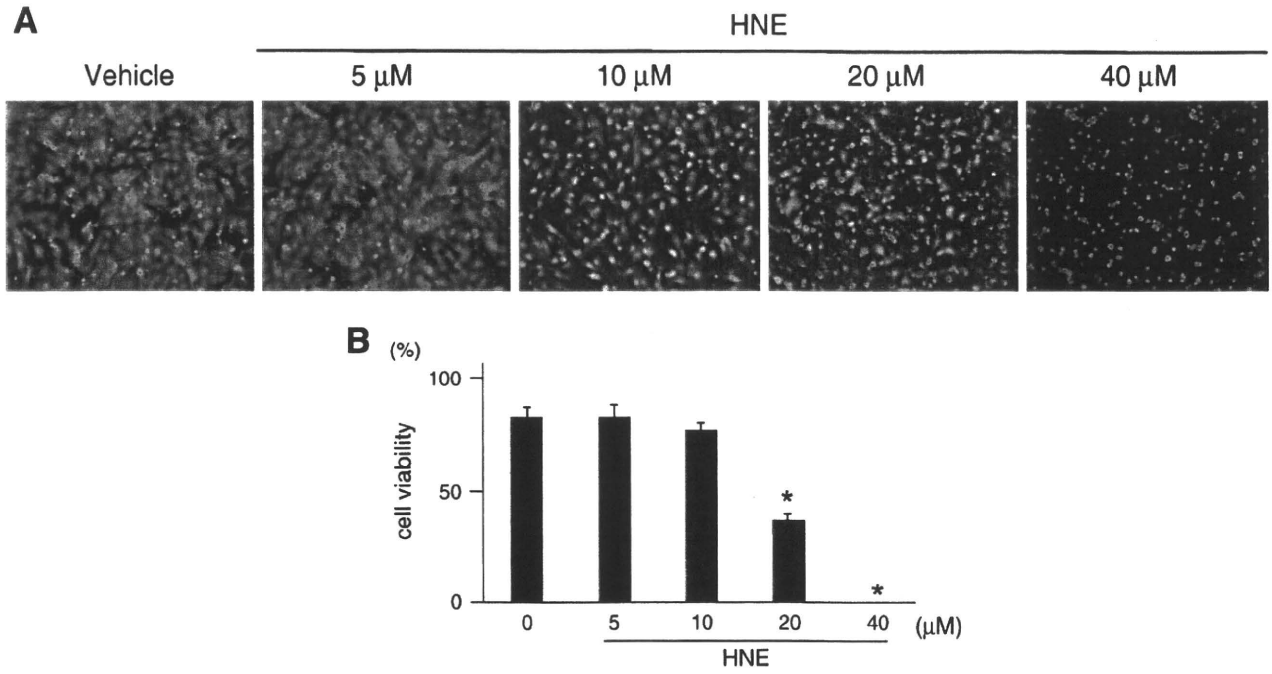

Fig. 1. 4-HNE causes cell death at higher concentrations but lacks cytotoxicity at lower concentrations. (A) Representative images of cardiomyocytes that were treated with different concentrations of 4-HNE. (B) Quantification of cell viability. Data shown are mean ± SEM ($n = 5$). *$P<0.05$ vs. vehicle-treated cardiomyocytes (unpaired Student's t-test).

3.2. Pretreatment with a sublethal concentration of 4-HNE protects cardiomyocytes against subsequent oxidative cell death induced by a high dosage of 4-HNE

To examine the effects of 4-HNE, cardiomyocytes were pretreated with either vehicle or 5 μM 4-HNE for 14 h, and then treated with cytotoxic concentrations of 4-HNE for 24 h. The viabilities of the vehicle-pretreated cardiomyocytes were 24.59% ± 4.31% for 20 μM 4-HNE and 15.42% ± 1.76% for 30 μM 4-HNE. Pretreatment with 5 μM 4-HNE significantly increased the cardiomyocyte viabilities to 72.09% ± 5.53% for 20 μM 4-HNE and 38.65% ± 4.12% for 30 μM 4-HNE (Fig. 2A, B).

3.3. 4-HNE induces antioxidant enzymes and GSH synthesis in cardiomyocytes

We examined the underlying molecular mechanisms responsible for the cytoprotective effect of 4-HNE on cardiomyocytes. 4-HNE treatment increased both the mRNA and protein expression levels of various antioxidant enzymes, including HO-1, catalase, Gsta2, Gclc, and xCT (Fig. 3A, B). The rate of glutathione (GSH) synthesis is determined primarily by Gclc activity and the availability of precursor amino acids, especially cysteine. Consistent with the increased levels of Gclc and xCT, the intracellular concentration of GSH was increased 1.45-fold in cardiomyocytes that were treated with 5 μM 4-HNE for 24 h, as compared to cells that were treated with vehicle (261.08 ± 19.35 μM/g vs. 179.89 ± 11.59 μM/g, respectively) (Fig. 3C).

3.4. Nrf2 plays a key role in the induction of stress responses

Nrf2 has been implicated as a key transcription factor that induces the expression of antioxidant genes. Under non-stress conditions, Nrf2 is bound to Kelch-like ECH-associated protein 1 (Keap1) in the cytoplasm. This complex directs Nrf2 polyubiquitination and degradation. During oxidative stress, Nrf2 is liberated from Keap1 and enters the nucleus, where it can form a heterodimer with the small Maf transcription factor Nrf2, to stimulate the expression of antioxidant response element (ARE)-containing genes [14]. Therefore, we investigated the possibility that Nrf2 accumulates in the nucleus after 4-HNE treatment. Cultured cardiomyocytes were treated with 4-HNE for 1 h, and nuclear extracts of these cells were subjected to immunoblotting. Nuclear accumulation of Nrf2 in response to 4-HNE treatment was observed (Fig. 4A).

To investigate whether Nrf2 signaling is important for the favorable response to 4-HNE, the cardiomyocytes were subjected to RNA interference to block Nrf2 expression and then stimulated with 4-HNE (5 μM) or vehicle for 6 h. Nrf2 silencing almost completely suppressed the 4-HNE-mediated increases in the expression levels of Gclc, xCT, and Gsta2. In contrast, Nrf2 silencing only modestly suppressed the 4-HNE-mediated increase in HO-1 expression (Fig. 4B). Therefore, we examined the possible involvement of Nrf2 in the observed increased in GSH level. Nrf2 silencing cells and control cells were treated with 4-HNE (5 μM) or vehicle for 14 h. Nrf2 silencing resulted in no appreciable cytotoxicity under these conditions (data not shown). The 4-HNE-mediated increase in GSH level was markedly suppressed in Nrf2 siRNA-treated cardiomyocytes, as compared to control siRNA-treated cardiomyocytes (115.98 ± 8.63 μM/mg vs. 213.43 ± 16.24 μM/mg, respectively) (Fig. 4C).

Next, we examined the effect of Nrf2 silencing on cardiomyocyte viabilities. Cardiomyocytes were treated with either Nrf2-specific siRNA or a control siRNA for 24 h, and then stimulated with 4-HNE (5 μM or 10 μM) for 24 h. Whereas neither 5 μM nor 10 μM 4-HNE was toxic for cardiomyocytes treated with the control siRNA (81.89% ± 2.95% for 5 μM 4-HNE; 71.97% ± 4.44% for 10 μM 4-HNE), Nrf2 silencing significantly decreased cardiomyocyte viability in the presence of 4-HNE (48.94% ± 3.30% for 5 μM 4-HNE; and 14.49% ± 1.40% for 10 μM 4-HNE) (Fig. 5A, B).

To examine the role of Nrf2 in the induction of protection mediated by 4-HNE, Nrf2-depleted cardiomyocytes were preincubated with 5 μM 4-HNE for 14 h, and then stimulated with 10 μM or 20 μM of 4-HNE for an additional 24 h. Preincubation with 5 μM 4-HNE for 14 h had no appreciable cytotoxic effect on either the Nrf2-wildtype or Nrf2-depleted cardiomyocytes. However, the viabilities of

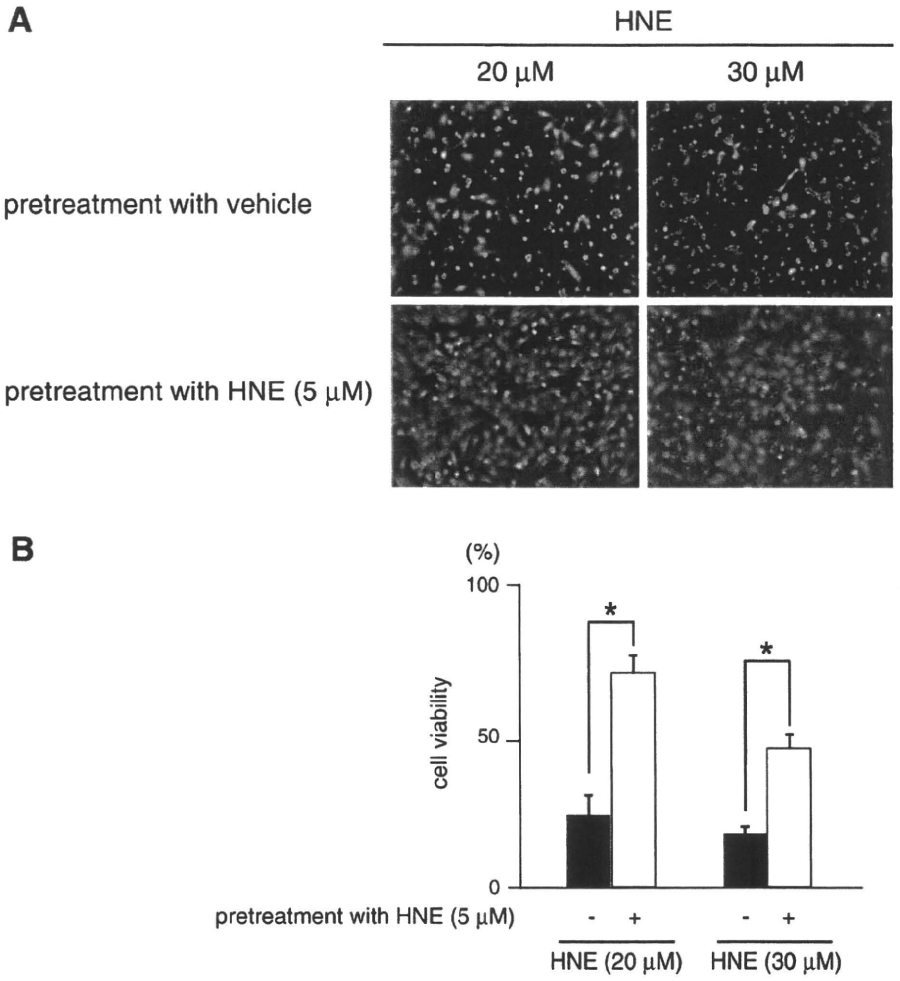

Fig. 2. Exposure to a sublethal concentration of 4-HNE enables cardiomyocytes to adapt to cytotoxic concentrations of 4-HNE. Cardiomyocytes were treated with either vehicle or 4-HNE (5 μM) for 14 h, and then incubated with a toxic concentration (20 μM or 30 μM) of 4-HNE for 24 h. (A) Representative images of cardiomyocytes that were treated with toxic concentrations of 4-HNE. (B) Quantification of cell viability. Data shown are mean ± SEM ($n = 5$). *$P<0.05$ vs. vehicle-pretreated cardiomyocytes (unpaired Student's t-test).

the Nrf2-depleted cardiomyocytes in 10 μM 4-HNE and 20 μM 4-HNE were 0.00% and 0.00%, respectively, while those of the control cells were 86.69% ± 3.49% and 71.18% ± 3.43%, respectively (Fig. 5C, D).

3.5. BSO treatment sensitizes cardiomyocytes to 4-HNE-induced cell death

To investigate whether GSH is an important factor in tolerance to 4-HNE, cardiomyocytes were incubated with 50 μM BSO, an inhibitor of GSH biosynthesis, in the presence or absence of 4-HNE (5 μM) for 14 h. BSO treatment decreased the intracellular GSH concentration from 162.47 ± 3.02 μM/mg (vehicle-treated cardiomyocytes) to 98.98 ± 12.13 μM/mg (BSO-treated cardiomyocytes). In addition, simultaneous 4-HNE treatment (5 μM) failed to increase the intracellular GSH levels of the BSO-treated cardiomyocytes (Fig. 6A). This concentration of BSO showed no appreciable effect on cardiomyocyte viability in the absence of 4-HNE, whereas it sensitized the cardiomyocytes to 4-HNE-induced death, as compared to the vehicle treatment. The viabilities of the vehicle-pretreated cardiomyocytes were 82.64% ± 3.07% for 5 μM 4-HNE and 72.61% ± 2.02% for 10 μM 4-HNE. Pretreatment with BSO significantly decreased the cardiomyocyte viabilities to 53.60 ± 2.79% for 5 μM 4-HNE and 35.16% ± 2.40% for 10 μM 4-HNE (Fig. 6B, C).

To examine the role of GSH biosynthesis in the induction of 4-HNE-mediated protection, cardiomyocytes were incubated with 5 μM 4-HNE in the presence of 50 μM BSO for 14 h, and then stimulated with 10 μM or 20 μM 4-HNE for an additional 24 h. The preincubation with 5 μM 4-HNE for 14 h had no appreciable cytotoxicity even in the presence of 50 μM BSO. However, the cardiomyocyte viabilities for treatment with 10 μM 4-HNE and 20 μM 4-HNE were 5.88% ± 0.46% and 0.00%, respectively, in the BSO-treated groups, and 88.52% ± 1.39% and 73.77% ± 1.60%, respectively, in the control groups (Fig. 6D, E).

3.6. 4-HNE pretreatment improves the functional recovery of Langendorff-perfused hearts after ischemia–reperfusion injury

The effect of 4-HNE treatment on function recovery after ischemia–reperfusion was studied in Langendorff-perfused mouse hearts. Mice were injected with either 4 mg/kg 4-HNE or vehicle (50 μl of saline) *via* the retro-orbital vein [12] [13], and 24 h later, the hearts were isolated and subjected to 25 min of total global ischemia, followed by 60 min of aerobic reperfusion. We selected 4 mg/kg 4-HNE as the optimal dosage based on a pilot study in which various amounts of 4-HNE were administered *via* the retro-orbital vein. We confirmed that sufficient reactive 4-HNE reaches the heart upon systemic administration within

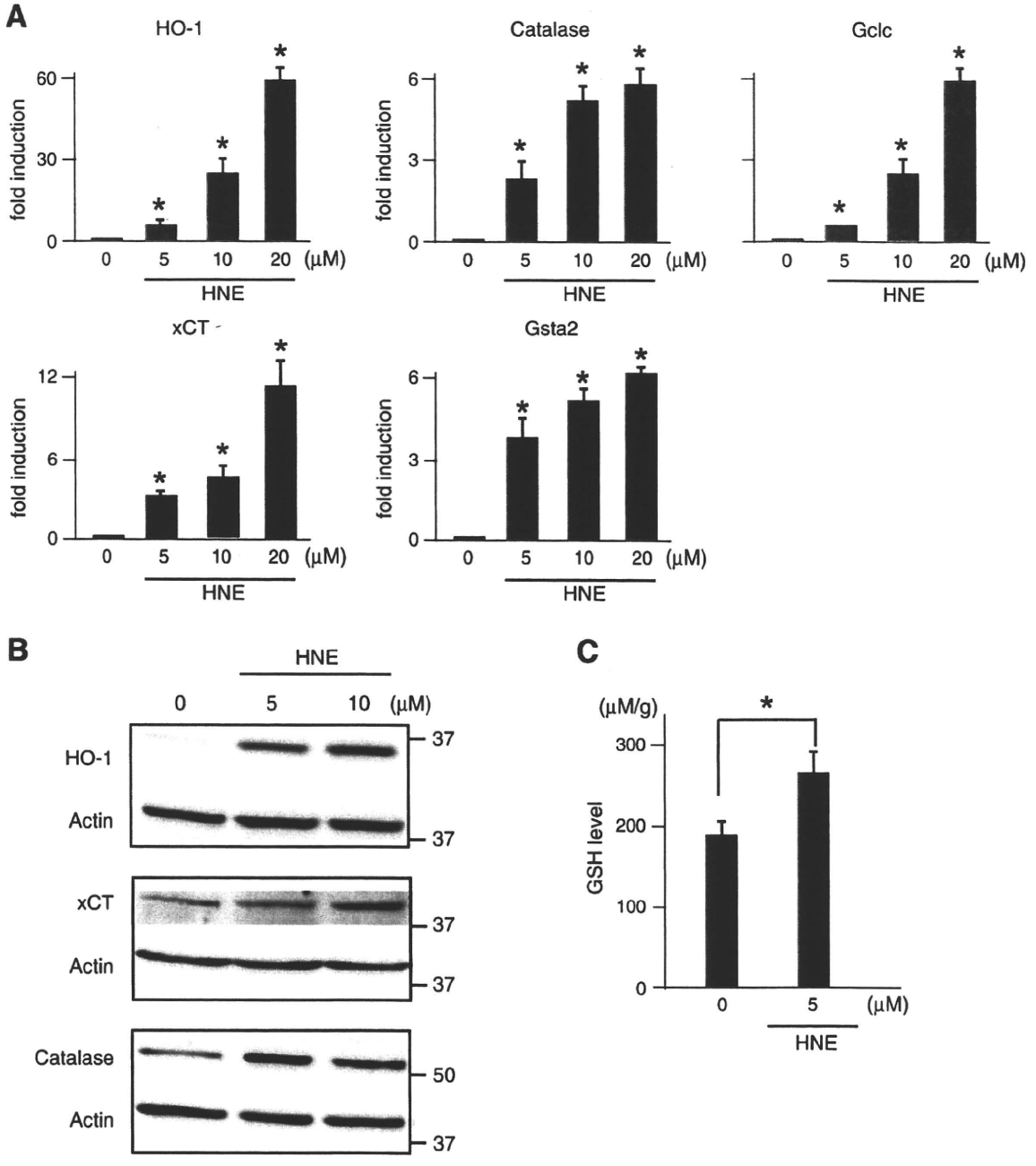

Fig. 3. 4-HNE increases the cardiomyocyte expression levels of antioxidant enzymes and GSH. (A) Cardiomyocytes were treated with different concentrations of 4-HNE (0, 5, 10, 20 μM) for 6 h. Antioxidant gene expression was determined by Q-PCR analysis. $n = 5$; $^*P<0.05$ vs. vehicle-treated cardiomyocytes. (B) Cardiomyocytes were treated with different concentrations of 4-HNE (0, 5, 10 μM) for 14 h. The antioxidant enzyme expression levels were determined by immunoblotting. (C) Cardiomyocytes were treated with 4-HNE for 24 h. The intracellular levels of GSH were measured using Bioxytech GSH/GSSG-412 (Oxis Research), based on the Tietze method; $n = 5$, $^*P<0.05$, compared to the vehicle-treated cardiomyocytes.

60 min (Supplemental Fig. 2) and activated Nrf2 in the hearts (Supplemental Fig. 3A). The administration of 4-HNE *via* the retro-orbital vein significantly upregulated the levels of mRNA for antioxidant enzymes (Supplemental Fig. 3B) and increased the GSH levels, as compared to vehicle-treated control hearts (237.41 ± 12.24 mM/g for the 4-HNE-treated group vs. 214.26 ± 4.89 mM/g for the control group; $n = 4$, $P<0.05$).

4-HNE pretreatment did not affect the cardiac parameters at baseline (data not shown), whereas it significantly improved the recovery of LVDP, positive dP/dt, and negative dP/dt, as compared to the control treatment (Fig. 7). Consistent with these findings, the level of total LDH release into the perfusate during reperfusion was significantly lower in the 4-HNE-pretreatment hearts than in the control hearts.

Next, we examined the changes in the levels of 4-HNE in the hearts using antibodies specific for 4-HNE adduct proteins. Despite the significant changes in cardiac gene expression and GSH content, we did not detect any difference in the levels of 4-HNE adduct proteins between the vehicle-treated and 4-HNE-treated hearts. Ischemia–reperfusion significantly increased the levels of 4-HNE adduct proteins in the Langendorff-perfused hearts. Consistent with the significant reduction

of infarct size, pretreatment with 4-HNE significantly attenuated the increase in 4-HNE adduct proteins during reperfusion injury (Supplemental Fig. 4).

3.7. 4-HNE treatment has no effect on the functional recovery of the left ventricle after ischemia–reperfusion in Langendorff-perfused Nrf2-knockout mouse hearts

To examine the role of Nrf2 in the cardioprotective effect of 4-HNE, Nrf2-knockout mice were injected i.v. with either 4 mg/kg 4-HNE or vehicle, and 24 h later, the hearts were isolated and subjected to the same ischemia–reperfusion protocol. There was no difference in LV function before the induction of ischemia between the hearts from the Nrf2-knockout mice and those from the wild-type control mice. 4-HNE pretreatment did not affect the cardiac parameters at baseline in the Nrf2-knockout mice (data not shown). 4-HNE pretreatment did not improve the recovery of LVDP or rate-pressure product during reperfusion of the Nrf2-knockout mouse hearts. Moreover, 4-HNE pretreatment did not attenuate the total LDH activity released into the perfusate during reperfusion (Fig. 8). Notably, 4-HNE pretreatment

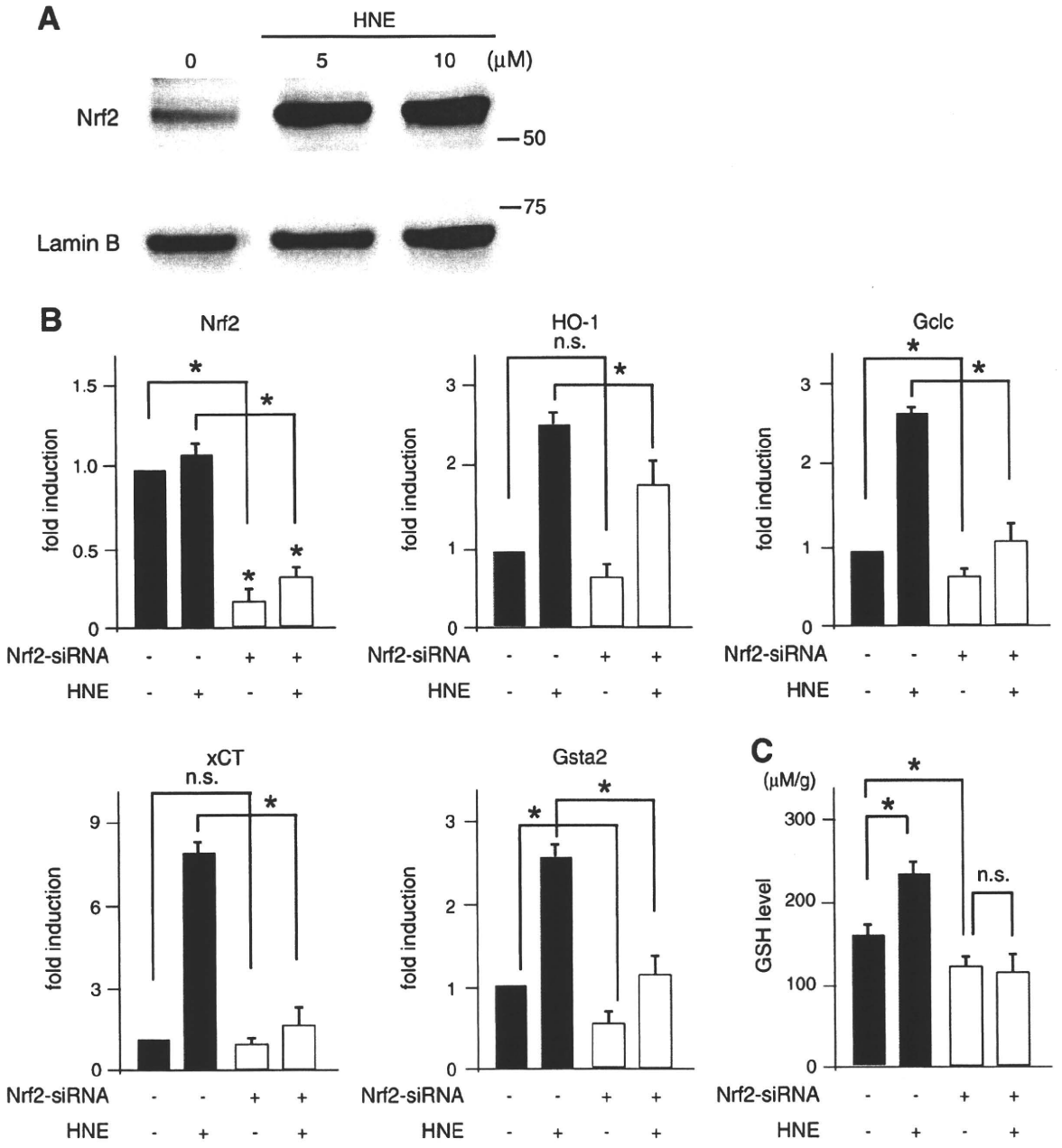

Fig. 4. Nrf2-dependent transcription is activated in 4-HNE-treated cardiomyocytes. (A) Cardiomyocytes were treated with sublethal concentrations of 4-HNE (0, 5, 10 μM) for 1 h. Nuclear extracts were subjected to SDS-PAGE, and Nrf2 was detected by immunoblotting. Membranes were stripped and reprobed with anti-Lamin B antibodies. (B) Cardiomyocytes were treated with either an Nrf2-specific siRNA or a control siRNA for 24 h, and then stimulated with 4-HNE (5 μM) for 6 h. Antioxidant gene expression was determined by Q-PCR analysis; $n=5$, $^*P<0.05$, compared to control siRNA-treated cardiomyocytes. (C) The intracellular levels of GSH were measured 14 h after 4-HNE (5 μM) treatment using Bioxytech GSH/GSSG-412 (Oxis Research), based on the Tietze method; $n=5$, $^*P<0.05$, compared to control siRNA-treated cardiomyocytes without 4-HNE stimulation.

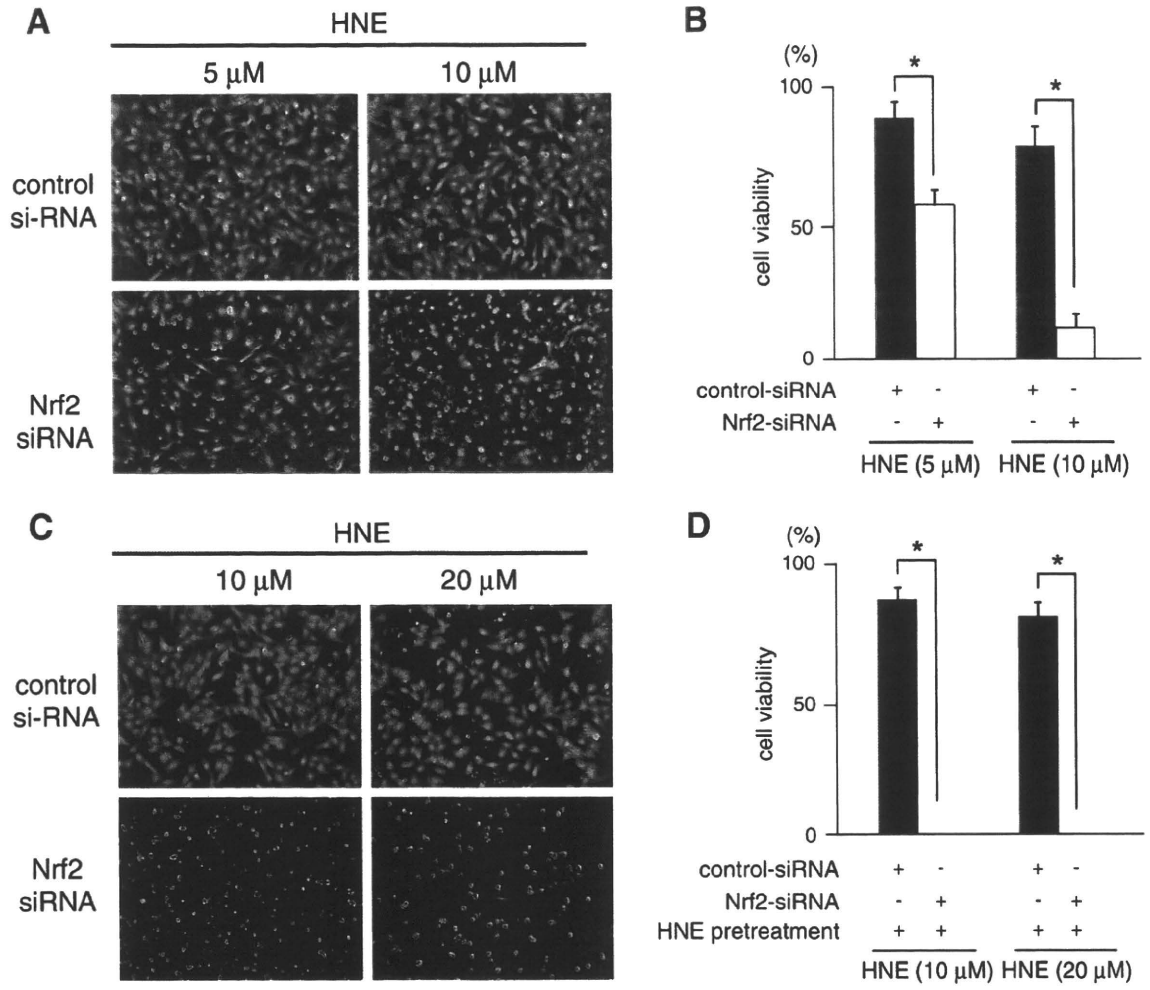

Fig. 5. Nrf2-deficient cardiomyocytes exhibit lower resistance to oxidative stress and the adaptive response to 4-HNE is completely abolished. Cardiomyocytes were treated with either Nrf2-specific siRNA or a control siRNA for 24 h, and then stimulated with 4-HNE (5 μM or 10 μM) for 24 h. (A) Representative images of cardiomyocytes after treatment with different concentrations of 4-HNE. (B) Quantification of cell viability. Data shown are mean ± SEM ($n = 5$). *$P<0.05$ vs. control siRNA-treated cardiomyocytes (unpaired Student's t-test). Nrf2-depleted cardiomyocytes were preincubated with 5 μM 4-HNE for 14 h, and then stimulated with 4-HNE (10 μM or 20 μM) for 24 h. (C) Representative images of cardiomyocytes after treatment with different concentrations of 4-HNE. (D) Quantification of cell viability. Data shown are mean ± SEM ($n = 5$). *$P<0.05$ vs. control siRNA-treated cardiomyocytes (unpaired Student's t-test).

increased the protein expression levels of xCT, GPX4, Gclc, Gsta, HO-1, and Catalase in the Nrf-2 wild-type hearts, but not in the Nrf2-knockout hearts (Supplemental Fig. 5).

4. Discussion

In addition to the pathogenic effects associated with oxidative stress, 4-HNE is considered to play an important role as a signal transduction molecule in stimulating the antioxidant defense network. This induction of stress-protective mechanisms is referred to as "stress-response hormesis" [9]. The present study provides insights into the clinical significance of stress-response hormesis induced by 4-HNE (Supplemental Fig. 7).

Hormesis is generally defined as a biphasic dose–response curve to a treatment that is beneficial at low levels but noxious at higher levels [15]. However, for practical reasons, most researchers in the fields of aging and molecular biology use a limited number of dosages within the optimal or hormetic zone when studying adaptive mechanisms. Thus, these researchers report hormetic effects without having to confirm the biphasic dose–response curve. This is certainly true for many examples of preconditioning. In the present study, we show a biphasic dose–response curve; 4-HNE induced cardiomyocyte death at higher concentrations (≥20 μM), whereas it had no appreciable cytotoxicity at lower concentrations (≤10 μM). Notably, a lower concentration of 4-HNE primed the cardiomyocytes for subsequent oxidative injury, thereby enabling the cells to adapt to cytotoxic concentrations of 4-HNE. Furthermore, we demonstrate that the administration of 4-HNE *via* the retro-orbital vein protects the heart against cell death induced by ischemia–reperfusion injury. 4-HNE pretreatment significantly attenuated the accumulation of 4-HNE adduct proteins during reperfusion. A growing body of evidence indicates that a brief ischemic insult in one organ releases endogenous factors that protect other organs against a prolonged ischemic insult [16]. This phenomenon is known as 'remote ischemic preconditioning'. The exact nature of signaling transduction from remote tissue to target organ remains to be fully elucidated. Aldehydes are more stable than their precursor ROS, which means that they can diffuse to sites at a distance from their site of injury. Aldehydes conjugate with receptive nucleophiles, such as glutathione. In the present study, we raise the possibility that aldehydes and/or their metabolites act as humoral mediators to mediate distant organ protection.

We show that Nrf2 is a key transcriptional regulator for 4-HNE-mediated establishment of antioxidative defenses, at least under acute conditions. These results are consistent with recent reports that

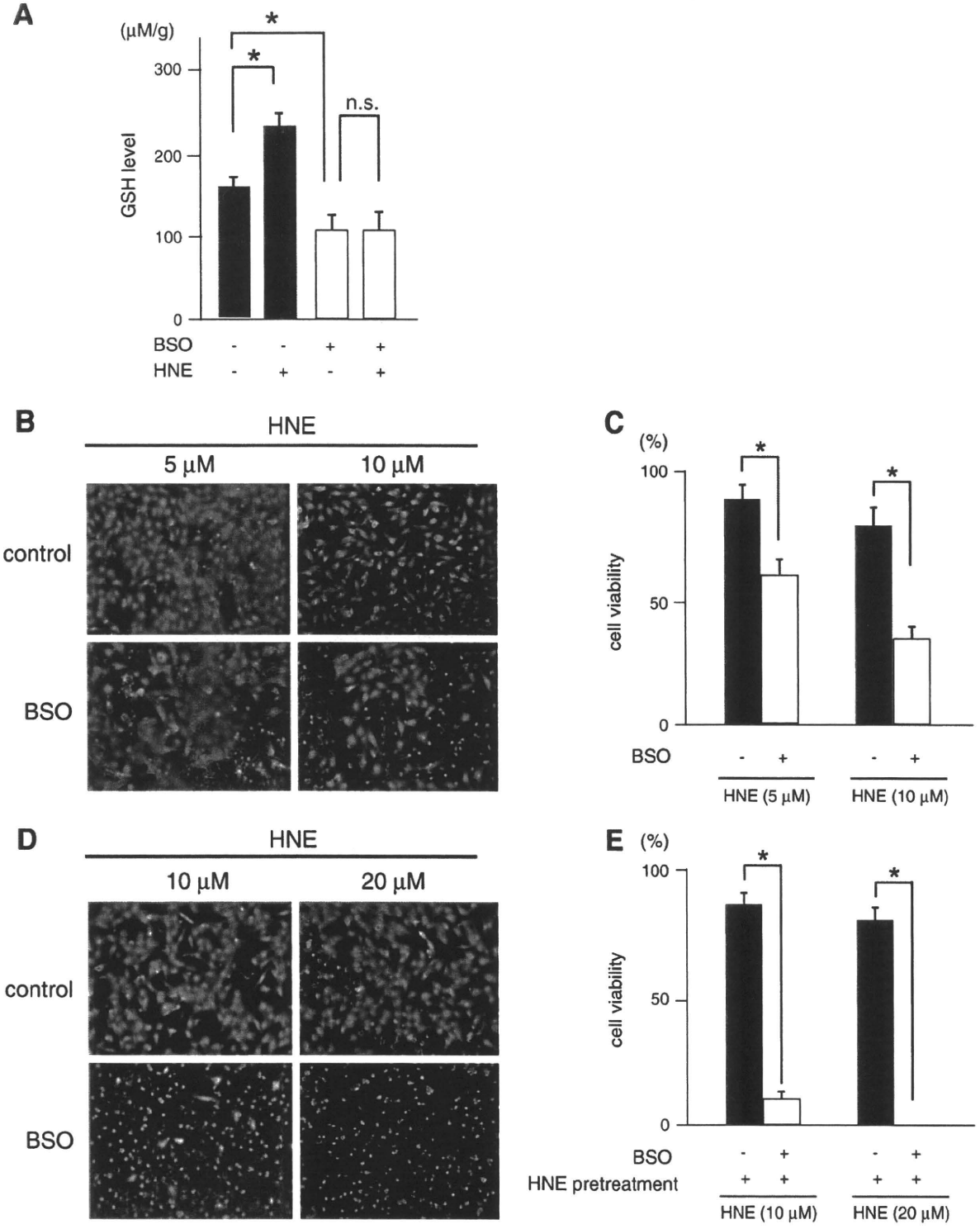

Fig. 6. Depletion of intracellular GSH using BSO renders cardiomyocytes less tolerant to 4-HNE and abolishes the 4-HNE-induced preconditioning effect. (A) Cardiomyocytes were incubated with 50 μM BSO in the presence or absence of 4-HNE (5 μM) for 14 h. The intracellular levels of GSH were measured using Bioxytech GSH/GSSG-412 (Oxis Research), based on the Tietze method; $n = 5$, $^*P < 0.05$, compared to BSO-untreated cardiomyocytes without 4-HNE stimulation. (B) Cardiomyocytes were incubated with 50 μM BSO, and then stimulated with 4-HNE for 24 h. Representative images of cardiomyocytes after treatment with 4-HNE. (C) Quantification of cell viability. Data shown are mean ± SEM ($n = 5$). $^*P < 0.05$ vs. BSO-untreated cardiomyocytes. (D) Cardiomyocytes were preconditioned with 4-HNE (5 μM) in the presence or absence of 50 μM BSO for 14 h, and then examined for tolerance to higher dosages (10 μM and 20 μM) of 4-HNE. Representative images of cardiomyocytes after treatment with 4-HNE. (E) Quantification of cell viability. Data shown are mean ± SEM ($n = 5$). $^*P < 0.05$ vs. 4-HNE-preconditioned cardiomyocytes without BSO treatment.

Nrf2 signaling plays an important role in 3H-1,2-dithiole-3-thione (D3T)- or H_2O_2-induced protection against oxidative injury to cardiomyocytes [17] [18]. Under unstressed conditions, Nrf2 is tethered to Keap1 in the cytoplasm. This complex directs Nrf2 polyubiquitination and degradation. During oxidative stress, Nrf2 is liberated from Keap1 and enters the nucleus, where it forms a

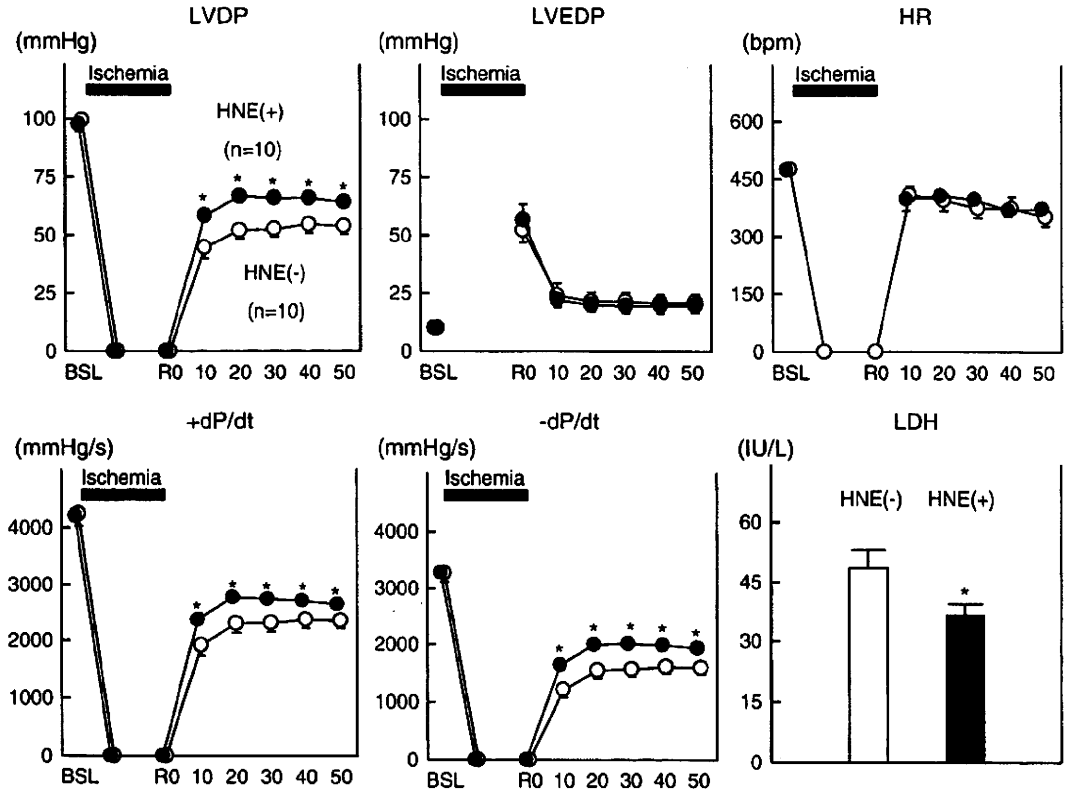

Fig. 7. 4-HNE treatment significantly improves the functional recovery of the left ventricle after ischemia-reperfusion in Langendorff-perfused hearts. The stock solution of 4-HNE was diluted with PBS, and a dose of 4 mg/kg HNE was administered via the retro-orbital vein 24 hours before sacrifice under anesthesia using diethyl ether. A vehicle solution (ethanol diluted with PBS) was administered in the same manner. Twenty-four hours later, the hearts were excised rapidly under deep anesthesia using pentobarbital and were immediately mounted on the Langendorff apparatus. Langendorff-perfused hearts were subjected to 25 min of total global ischemia, followed by aerobic reperfusion. LVDP, Recovery of left ventricular developing pressure; LVEDP, diastolic pressure; HR, heart rate; +/−dP/dt, peak positive/negative dP/dt; RPP, rate pressure product. *$P<0.05$ for HNE-preconditioned hearts ($n=10$) vs. control hearts ($n=10$) (unpaired Student's t-test).

heterodimer with the small Maf transcription factor Nrf2, to induce the expression of genes for proteins that function as antioxidants and enzymes that are involved in phase II detoxification and glutathione biosynthesis [14]. The mechanism by which 4-HNE induces the nuclear accumulation of Nrf2 remains to be clarified. Specific cysteine residues (Cys273/Cys288) in the Keap1 protein are known to act as a sensor for oxidative stress, and modification of these residues leads to a conformational change in Keap1, with consequent release of Nrf2 [19]. 4-HNE induces a conformational change in Keap1 directly *via* adduct formation or indirectly by increasing the production of mitochondrial ROS [20].

There is accumulating evidence that the myocardial GSH content influences susceptibility to ischemia–reperfusion injury [21]. N-acetylcysteine and γ-glutamyl-cysteine ethyl ester, which are precursors in glutathione biosynthesis, significantly attenuate myocardial ischemia–reperfusion injury when administered before reperfusion [22]. In contrast, glutathione depletion exacerbates myocardial ischemia–reperfusion injury [21,23]. We show that the stimulation of cellular GSH biosynthesis through the up-regulation of GCL, a rate-limiting enzyme in GSH biosynthesis, plays a crucial role in 4-HNE-mediated cardioprotection *via* Nrf2 activation. Reduction of the GSH content to about 100 μM/g by either Nrf2-siRNA or BSO (a GCL inhibitor) sensitized the cardiomyocytes to 4-HNE-induced death and completely abolished the cardioprotective effect of a low dose of 4-HNE.

In addition to Nrf2, activating transcription factor 4 (ATF4) is also activated following the induction of oxidative stress and GSH biosynthesis [24]. Recently, we reported that life-long mitochondrial oxidative stress increases the phosphorylation levels of the α-subunit of translation initiation factor 2 (eIF2α) [25]. Phosphorylation of eIF2α inhibits general protein synthesis, although it specifically stimulates the translation of ATF4. ATF4 stimulates the expression of genes that encode enzymes that are involved in serine biosynthesis, while it does not stimulate the expression of GCL. Serine is a precursor of glycine and cysteine, both of which are needed for the biosynthesis of GSH. ATF4 also stimulates the expression of the solute-like carrier family of amino acid transporters. Thus, ATF4 activates GSH biosynthesis by providing the amino acids necessary for glutathione biosynthesis.

The rate of GSH synthesis is determined primarily by GCL activity and the availability of precursor amino acids. In the acute setting, Nrf-2-dependent induction of GCL expression mainly contributes to the enhanced production of GSH, thereby replenishing the intracellular GSH pool. However, once the intracellular GSH is recovered to normal levels, GCL activity is subject to feedback inhibition by GSH. To maintain in the long-term the increased levels of GSH so as to re-establish homeostasis under persistent oxidative stress, cardiomyocytes shift their glucose metabolism from mitochondrial oxidative energy production to the generation of reducing equivalents (NADPH or GSH) in the cytosol by activating the pentose phosphate pathway and amino acid metabolism *via* an ATF4-dependent mechanism [25]. Thus, Nrf2 and ATF4 appear to act in a co-ordinated manner to regulate glutathione biosynthesis and the glutathione redox cycle at different time-points [26].

Although the baseline expression levels of catalase, Gclc, and Gsta were suppressed by up to 50% in the Nrf2-knockout hearts, as compared to the wild-type hearts (Zhang and Sano, unpublished observation), the Nrf2-knockout hearts were phenotypically normal under the unstressed condition. However, the preconditioning effect of 4-HNE was

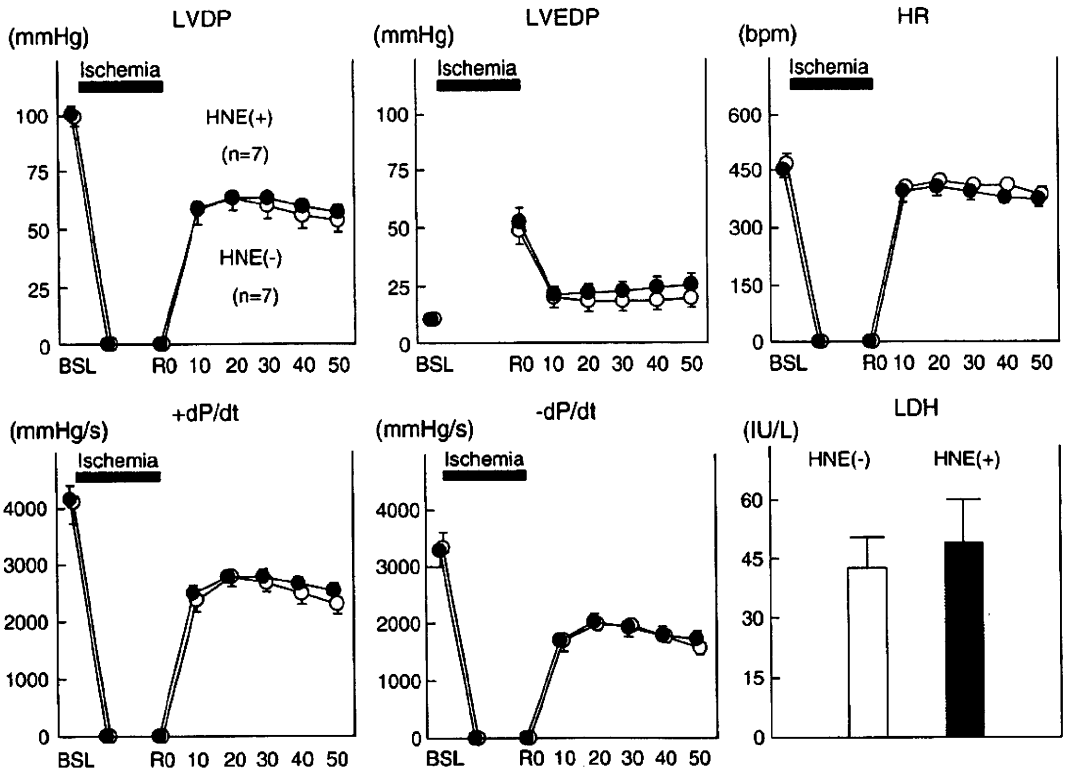

Fig. 8. 4-HNE treatment has no effect on the functional recovery of the left ventricle after ischemia–reperfusion in Langendorff-perfused Nrf2-knockout mouse hearts. 4-HNE (4 mg/kg) was injected into the ocular vein of each mouse. Langendorff-perfused hearts were subjected to 25 min of total global ischemia, followed by aerobic reperfusion. LVDP, Recovery of left ventricular developing pressure; LVEDP, diastolic pressure; HR, heart rate; +/−dP/dt, peak positive/negative dP/dt; RPP, rate pressure product. *$P<0.05$ for HNE-preconditioned ($n=7$) vs. control hearts ($n=7$) (unpaired Student's t-test).

completely absent in the Nrf2-knockout hearts. These results indicate that either Nrf2 is dispensable or that the Nrf2 defect is completely compensated for under the unstressed condition but is indispensable for the acute adaptive response under conditions of stress. Consistent with this notion, Nrf2-knockout hearts are prone to progression to terminal heart failure in response to pressure-overload by TAC [27]. Interestingly, the recovery of positive and negative dP/dt during early reperfusion was better in the Nrf2-knockout hearts than in the Nrf2-wildtype hearts (20 min of reperfusion and 10, 20, and 30 min of reperfusion, respectively) (Supplemental Fig. 4). The recovery of LVDP during early reperfusion tended to be better in Nrf2-KO mice, although the difference between Nrf2-wild-type and Nrf2-knockout mice was not statistically significant. These results strongly suggest that a compensatory mechanism against oxidative stress is stimulated in Nrf2-KO mice. However, the cardioprotection observed in the Nrf2-knockout mice was transient, and the recovery of LV function was similar in the two groups during late reperfusion (Supplemental Fig. 6). In addition, the finding that there was no difference in the total LDH activity released into the perfusate during reperfusion indicates that the extent of irreversible damage after ischemia–reperfusion is equivalent in Nrf2-wild-type and Nrf2-knockout mice, at least in these Langendorff-perfused hearts. 4-HNE pretreatment significantly improved the recovery of LV function during overall reperfusion, and attenuated LDH release during reperfusion in Nrf2-wildtype mice. Cardiac Nrf-2 was activated in the heart 60 min after the injection of 4-HNE via the retro-orbital vein. Both the up-regulation of cardiac anti-oxidant enzymes and the cardioprotection afforded by 4-HNE pretreatment were completely abrogated in the Nrf2- knockout mice. Therefore, we conclude that Nrf2 is essential for 4-HNE-induced cardioprotection, despite the differences in the patterns of LV functional recovery observed between Nrf2-wildtype and Nrf2-knockout mice. The mechanism by which Nrf2- knockout mice manifest improved LV function during early reperfusion remains unknown.

4-HNE is highly reactive so that most of 4-HNE may undergo nucleophilic addition reactions with electron-rich centers particularly non-protein and protein thiols and amines in the blood. Thus, we examined whether sufficient reactive 4-HNE reaches the heart upon systemic administration using antibodies specific for 4-HNE adduct proteins and showed that the level of 4-HNE in the heart was increased at 60 min after the administration of 4-HNE via the retro-orbital vein. We also demonstrated that cardiac Nrf2 is activated at 60 min after systemic administration of 4-HNE. We concluded that 4-HNE or 4-HNE conjugate metabolite can reaches the heart upon systemic administration and stimulate intracellular signaling in the heart. Notably, not only free 4-HNE but also 4-HNE conjugate metabolite can stimulate intracellular signaling and increased cell growth in cultured vascular smooth muscle cells [28].

Several studies have suggested that the generation of aldehydes, such as 4-HNE, contributes to much of the damage induced by ROS [29]. The present study intriguingly shows that a sublethal concentration of 4-HNE protects cardiomyocytes from ischemia–reperfusion injury. An improved understanding of the dual roles of 4-HNE would facilitate the design of novel strategies for cardioprotection against oxidative stress [30].

Disclosures

None.

Sources of funding

This work was supported by the Japan-China Medical Association (to Y.Z.) and by a PRESTO (Metabolism and Cellular Function) grant from the Japanese Science and Technology Agency (to M.S.).

Acknowledgments

The authors thank the Japan-China Medical Association and the Japan Foundation for giving Y. Zhang the opportunity to join our laboratory. The authors thank Y. Miyake, H. Shiozawa, M. Abe, and M. Doi for technical assistance. M. Sano and M. Suematsu are core members of the Global Center of Excellence (GCOE) for Human Metabolomics Systems Biology at MEXT.

Appendix A. Supplementary data

Supplementary data associated with this article can be found, in the online version, at doi:10.1016/j.yjmcc.2010.05.011.

References

[1] Conklin D, Prough R, Bhatanagar A. Aldehyde metabolism in the cardiovascular system. Mol Biosyst 2007 Feb;3(2):136–50.
[2] Watson AD, Leitinger N, Navab M, Faull KF, Horkko S, Witztum JL, et al. Structural identification by mass spectrometry of oxidized phospholipids in minimally oxidized low density lipoprotein that induce monocyte/endothelial interactions and evidence for their presence in vivo. J Biol Chem 1997 May 23;272 (21):13597–607.
[3] Liu Q, Raina AK, Smith MA, Sayre LM, Perry G. Hydroxynonenal, toxic carbonyls, and Alzheimer disease. Mol Aspects Med Aug-Oct 2003;24(4–5):305–13.
[4] Chen CH, Budas GR, Churchill EN, Disatnik MH, Hurley TD, Mochly-Rosen D. Activation of aldehyde dehydrogenase-2 reduces ischemic damage to the heart. Science 2008 Sep 12;321(5895):1493–5.
[5] Honarbakhsh S, Schachter M. Vitamins and cardiovascular disease. Br J Nutr 2009 Apr;101(8):1113–31.
[6] Uchida K, Shiraishi M, Naito Y, Torii Y, Nakamura Y, Osawa T. Activation of stress signaling pathways by the end product of lipid peroxidation. 4-hydroxy-2-nonenal is a potential inducer of intracellular peroxide production. J Biol Chem 1999 Jan 22;274(4):2234–42.
[7] Dickinson DA, Iles KE, Watanabe N, Iwamoto T, Zhang H, Krzywanski DM, et al. 4-hydroxynonenal induces glutamate cysteine ligase through JNK in HBE1 cells. Free Radic Biol Med 2002 Oct 1;33(7):974.
[8] Chen ZH, Saito Y, Yoshida Y, Sekine A, Noguchi N, Niki E. 4-Hydroxynonenal induces adaptive response and enhances PC12 cell tolerance primarily through induction of thioredoxin reductase 1 via activation of Nrf2. J Biol Chem 2005 Dec 23;280(51):41921–7.
[9] Gems D, Partridge L. Stress-response hormesis and aging: "that which does not kill us makes us stronger". Cell Metab 2008 Mar;7(3):200–3.
[10] Iida K, Itoh K, Kumagai Y, Oyasu R, Hattori K, Kawai K, et al. Nrf2 is essential for the chemopreventive efficacy of oltipraz against urinary bladder carcinogenesis. Cancer Res 2004 Sep 15;64(18):6424–31.
[11] Tokudome S, Sano M, Shinmura K, Matsuhashi T, Morizane S, Moriyama H, et al. Glucocorticoid protects rodent hearts from ischemia/reperfusion injury by activating lipocalin-type prostaglandin D synthase-derived PGD2 biosynthesis. J Clin Invest 2009 Jun;119(6):1477–88.
[12] Hyafil F, Vergely C, Du Vignaud P, Grand-Perret T. In vitro and in vivo reversal of multidrug resistance by GF120918, an acridonecarboxamide derivative. Cancer Res 1993 Oct 1;53(19):4595–602.
[13] Kettner A, Kumar L, Anton IM, Sasahara Y, de la Fuente M, Pivniouk VI, et al. WIP regulates signaling via the high affinity receptor for immunoglobulin E in mast cells. J Exp Med 2004 Feb 2;199(3):357–68.
[14] Motohashi H, Yamamoto M. Nrf2-Keap1 defines a physiologically important stress response mechanism. Trends Mol Med 2004 Nov;10(11):549–57.
[15] Calabrese EJ, Baldwin LA, Holland CD. Hormesis: a highly generalizable and reproducible phenomenon with important implications for risk assessment. Risk Anal 1999 Apr;19(2):261–81.
[16] Kharbanda RK, Nielsen TT, Redington AN. Translation of remote ischaemic preconditioning into clinical practice. Lancet 2009 Oct 31;374(9700):1557–65.
[17] Zhu H, Jia Z, Misra BR, Zhang L, Cao Z, Yamamoto M, et al. Nuclear factor E2-related factor 2-dependent myocardiac cytoprotection against oxidative and electrophilic stress. Cardiovasc Toxicol Summer 2008;8(2):71–85.
[18] Purdom-Dickinson SE, Lin Y, Dedek M, Morrissy S, Johnson J, Chen QM. Induction of antioxidant and detoxification response by oxidants in cardiomyocytes: evidence from gene expression profiling and activation of Nrf2 transcription factor. J Mol Cell Cardiol 2007 Jan;42(1):159–76.
[19] Kobayashi A, Kang MI, Watai Y, Tong KI, Shibata T, Uchida K, et al. Oxidative and electrophilic stresses activate Nrf2 through inhibition of ubiquitination activity of Keap1. Mol Cell Biol 2006 Jan;26(1):221–9.
[20] Hill BG, Dranka BP, Zou L, Chatham JC, Darley-Usmar VM. Importance of the bioenergetic reserve capacity in response to cardiomyocyte stress induced by 4-hydroxynonenal. Biochem J 2009 Nov 15;424(1):99–107.
[21] Singh A, Lee KJ, Lee CY, Goldfarb RD, Tsan MF. Relation between myocardial glutathione content and extent of ischemia–reperfusion injury. Circulation 1989 Dec;80(6):1795–804.
[22] Hoshida S, Kuzuya T, Yamashita N, Nishida M, Kitahara S, Hori M, et al. gamma-Glutamylcysteine ethyl ester for myocardial protection in dogs during ischemia and reperfusion. J Am Coll Cardiol 1994 Nov 1;24(5):1391–7.
[23] Blaustein A, Deneke SM, Stolz RI, Baxter D, Healey N, Fanburg BL. Myocardial glutathione depletion impairs recovery after short periods of ischemia. Circulation 1989 Nov;80(5):1449–57.
[24] Harding HP, Zhang Y, Zeng H, Novoa I, Lu PD, Calfon M, et al. An integrated stress response regulates amino acid metabolism and resistance to oxidative stress. Mol Cell 2003 Mar;11(3):619–33.
[25] Endo J, Sano M, Katayama T, Hishiki T, Shinmura K, Morizane S, et al. Metabolic remodeling induced by mitochondrial aldehyde stress stimulates tolerance to oxidative stress in the heart. Circ Res 2009 Nov 20;105(11):1118–27.
[26] Sano M, Fukuda K. Activation of mitochondrial biogenesis by hormesis. Circ Res 2008 Nov 21;103(11):1191–3.
[27] Li J, Ichikawa T, Villacorta L, Janicki JS, Brower GL, Yamamoto M, et al. Nrf2 protects against maladaptive cardiac responses to hemodynamic stress. Arterioscler Thromb Vasc Biol Jul 10 2009.
[28] Ramana KV, Bhatnagar A, Srivastava S, Yadav UC, Awasthi S, Awasthi YC, et al. Mitogenic responses of vascular smooth muscle cells to lipid peroxidation-derived aldehyde 4-hydroxy-trans-2-nonenal (HNE): role of aldose reductase-catalyzed reduction of the HNE-glutathione conjugates in regulating cell growth. J Biol Chem 2006 Jun 30;281(26):17652–60.
[29] Veronneau M, Comte B, Des Rosiers C. Quantitative gas chromatographic-mass spectrometric assay of 4-hydroxynonenal bound to thiol proteins in ischemic/reperfused rat hearts. Free Radic Biol Med 2002 Nov 15;33(10):1380–8.
[30] Hill BG, Bhatnagar A. Beyond reactive oxygen species: aldehydes as arbitrators of alarm and adaptation. Circ Res 2009 Nov 20;105(11):1044–6.

Am J Physiol Heart Circ Physiol 299: H1795–H1804, 2010.
First published September 17, 2010; doi:10.1152/ajpheart.00001.2010.

Increased C-reactive protein expression exacerbates left ventricular dysfunction and remodeling after myocardial infarction

Toshiyuki Takahashi, Toshihisa Anzai, Hidehiro Kaneko, Yoshinori Mano, Atsushi Anzai, Toshiyuki Nagai, Takashi Kohno, Yuichiro Maekawa, Tsutomu Yoshikawa, Keiichi Fukuda, and Satoshi Ogawa

Division of Cardiology, Department of Medicine, Keio University School of Medicine, Tokyo, Japan

Submitted 4 January 2010; accepted in final form 15 September 2010

Takahashi T, Anzai T, Kaneko H, Mano Y, Anzai A, Nagai T, Kohno T, Maekawa Y, Yoshikawa T, Fukuda K, Ogawa S. Increased C-reactive protein expression exacerbates left ventricular dysfunction and remodeling after myocardial infarction. *Am J Physiol Heart Circ Physiol* 299: H1795–H1804, 2010. First published September 17, 2010; doi:10.1152/ajpheart.00001.2010.—We previously reported serum C-reactive protein (CRP) elevation after acute myocardial infarction (MI) to be associated with adverse outcomes including cardiac rupture, left ventricular (LV) remodeling, and cardiac death. Experimental studies have indicated that CRP per se has various biological actions including proinflammatory and proapoptotic effects, suggesting a pathogenic role of CRP in the post-MI remodeling process. We tested the hypothesis that increased CRP expression would exacerbate adverse LV remodeling after MI via deleterious effects of CRP. Transgenic mice with human CRP expression (CRP-Tg) and their transgene-negative littermates (control) underwent left coronary artery ligation. There was no apparent difference in phenotypic features between CRP-Tg and control mice before MI. Although mortality and infarct size were similar in the two groups, CRP-Tg mice showed more LV dilation and worse LV function with more prominent cardiomyocyte hypertrophy and fibrosis in the noninfarcted regions after MI than controls. Histological evaluation conducted 1 wk post-MI revealed a higher rate of apoptosis and more macrophage infiltration in the border zones of infarcted hearts from CRP-Tg mice in relation to increased monocyte chemotactic protein (MCP)-1 expression and matrix metalloproteinase (MMP)-9 activity. Increased CRP expression exacerbates LV dysfunction and promotes adverse LV remodeling after MI in mice. The deleterious effect of CRP on post-MI LV remodeling may be associated with increased apoptotic rates, macrophage infiltration, MCP-1 expression, and MMP-9 activity in the border zone.

macrophage; apoptosis

EARLY REVASCULARIZATION AND pharmacological therapy have been used to improve clinical outcomes in patients with acute myocardial infarction (MI). However, in some instances, particularly in those in which myocardial ischemic damage is too severe and extensive to allow salvage, adverse left ventricular (LV) remodeling develops following MI. This deleterious remodeling is characterized by progressive LV dilation and depressed LV function. In the long-term, the development of LV remodeling leads to detrimental outcomes such as congestive heart failure and lethal arrhythmias. Although the precise mechanisms underlying adverse LV remodeling remain to be determined, the inflammatory response to myocardial tissue damage plays a pivotal role in the pathophysiology of the remodeling process (8).

C-reactive protein (CRP) is a major acute-phase inflammatory reactant produced predominantly in the liver. We previously reported that marked serum CRP elevation after acute MI is associated with adverse outcomes such as cardiac rupture, LV remodeling, LV mural thrombosis, and cardiac death (2, 3, 29). In addition, the CRP level in the acute phase of MI is a powerful independent marker of heart failure and long-term mortality (28). Although the CRP level is reportedly a significant risk factor for cardiovascular disease (23, 24), CRP has been regarded as simply a prognostic marker in clinical settings. However, recent experimental studies have indicated that CRP per se has various biological actions, including proinflammatory, thrombogenic, atherogenic, and proapoptotic effects (6, 7, 9, 10, 22, 26, 32, 33), suggesting a pathogenic role of CRP in the inflammatory response and myocardial tissue damage associated with LV remodeling after MI. Therefore, we hypothesized that increased CRP expression would have deleterious effects on adverse LV remodeling after MI.

To examine the direct in vivo involvement of CRP in the adverse remodeling process following MI, we generated transgenic mice with human CRP expression (CRP-Tg). Large anterior wall MIs were then induced in CRP-Tg mice and their transgene-negative littermates. We assessed survival, infarct size, and LV size and function after MI. We then sought to determine the mechanisms by which increased CRP expression might accelerate adverse LV remodeling after MI.

METHODS

Generation and characterization of CRP-Tg mice. The study protocol was approved by the Institutional Animal Care and Use Committee at Keio University School of Medicine (No. 050015), and animal use and care were in accordance with Institutional and National Institutes of Health (NIH) guidelines. To generate transgenic mice with ubiquitous expression of human CRP, human CRP cDNA was inserted into the unique *Eco*RI site between the CAG (modified chicken β-actin promoter with CMV-IE enhancer) promoter and 3′-flanking sequence of the rabbit β-globin gene of the pCAGGS expression vector 4797 (Fig. 1*A*). The pronuclei of fertilized eggs from hyperovulated C57BL/6 mice were microinjected with this DNA construct. Founder animals were identified and crossbred with wild-type mice of the same strain. Gene presence was confirmed using genomic DNA purified from clipped tail tips (Fig. 1*B*); gene expression in the heart was confirmed by real-time RT-PCR with primers for human CRP (forward: GCTGGTTATTGTGCTGTCTC; reverse: CAGTTCAGGACATTAGGACTGAAG). Protein expression of human CRP in the heart was also confirmed by Western blotting of LV homogenates with antibodies recognizing human CRP (Sigma-Aldrich, St. Louis, MO; Fig. 1*C*). Human CRP expression in various organ tissues, including heart, lung, and liver, was determined by

Address for reprint requests and other correspondence: T. Anzai, Div. of Cardiology, Dept. of Medicine, Keio Univ. School of Medicine, 35 Shinanomachi, Shinjuku-ku, Tokyo 160-8582, Japan (e-mail: anzai@cpnet.med.keio.ac.jp).

immunohistochemistry (Fig. 1*D*). Blood sampling was taken, and the serum was stored at −80°C when animals were euthanized. Serum CRP levels were measured by latex agglutination immunoassay using the Nanopia CRP kit (Sekisui Medical, Tokyo, Japan). The detection limit of this assay was 0.1 ml/dL. Blood pressures were measured in awake animals by the tail-cuff method using the BP-98A system (Softron; Tokyo, Japan). Mice were housed with free access to food and water and exposed to 12-h:12-h light-dark cycles.

MI. Male CRP-Tg mice (3 to 4 mo old; $n = 59$) and their age-matched, male transgene-negative littermates (control; $n = 63$) were used for the study. MI was induced by permanent ligation of the left coronary artery as described previously (13, 30). Briefly, mice were anesthetized with ketamine and xylazine, intubated, and connected to a rodent ventilator. The chest cavity was opened through the fourth intercostal space to expose the heart. Suture (7-0 silk) was tied around the proximal left coronary artery. Complete occlusion of the vessel was confirmed by the presence of myocardial blanching in the perfusion bed, and subsequently by histological assessment.

Survival study. MIs were induced in the CRP-Tg and control mice in a randomized, blinded fashion. This study was designed to determine the 5-wk survival of mice following MI; therefore, mice that did not survive the surgical procedure were not included in the analysis.

Histology. After hearts were arrested in diastole, excised, and rinsed with saline, they were fixed in Formalin and embedded in paraffin. The sections from apex, mid-LV, and base were stained with hematoxylin and eosin and Masson's trichrome. Infarct size was determined as the mean percent of infarct lengths divided by total LV circumferences in the three sections. Myocyte hypertrophy in the noninfarcted septum was assessed by measuring the mean myocyte cross-sectional area. The percent area of fibrosis within the remote and MI regions of the LV was also computed. In a subset of mice euthanized at 1 and 5 wk after MI, the atria and right ventricle were removed from the heart and the LV was opened by a long-axis incision. The LV was then laid flat on the plate. The endocardial and epicardial surfaces were photographed by a digital camera. Infarct size was measured as the ratio of infarct area to total LV area by planimetry as previously described (4). Infarct size was also assessed in a subgroup of animals euthanized at 24 h after MI to avoid differences in hypertrophy of the noninfarcted wall that might result from differences in human CRP expression. Hearts were excised and immersed in 1% agarose and sectioned perpendicular to the long axis into 1-mm-thick slices and stained with 1.0% 2,3,5-triphenyltetrazolium chloride (TTC) for 10 min at 37°C to delineate the infarct area from the noninfarcted viable area. Each slice was weighed and photographed, and the LV area and the area of infarction for each slice were determined by planimetry as described previously (30).

Echocardiography. Echocardiography was performed with a 12-MHz probe (EnVisor; Philips Medical Systems, Andover, MA) in mice before MI and 1 or 5 wk after MI. Animals were anesthetized with an intraperitoneal injection of tribromoethanol (125 μg/g). A parasternal short-axis view was obtained as a guide for LV M-mode imaging at the papillary muscle level. LV dimensions, including end-diastole diameter, end-systole diameter, and wall thickness, were measured using the leading-edge method on three consecutive cardiac cycles. The LV ejection fraction (EF) was calculated using the area-length method as described previously (30).

Hemodynamics. LV pressure was measured in intact mice 5 wk after MI ($n = 10$ for the control group; $n = 9$ for the CRP-Tg group). Mice were anesthetized with an intraperitoneal injection of pentobarbital sodium (80 μg/g) and connected to a rodent ventilator after endotracheal intubation. A 1.4F micromanometer catheter (Millar Instruments, Houston, TX) was inserted via the right carotid artery and advanced into the LV. Peak rates of LV pressure development (LV $+dP/dt$) and relaxation (LV $-dP/dt$) were measured using analysis software (PowerLab; ADInstruments, Colorado Springs, CO). Ten sequential beats were averaged for each measurement.

TUNEL staining. To evaluate the extent of apoptosis in infarcted hearts, TUNEL assays were performed on sectioned LV samples using the CardioTACS In Situ Apoptosis Detection Kit (R&D Systems, Minneapolis, MN) as previously described (30). Images of six to eight contiguous sections across the LV wall were obtained at the midventricle level to measure the number of TUNEL-positive cardiac myocyte nuclei in the noninfarcted remote, peri-infarct border, and infarct zones. Digital images were evaluated using NIH Image to count TUNEL-positive stained nuclei and the total number of nuclei in a nuclease pretreated section from the same region. The area of each section was planimetered to calculate the average density of nuclei (nuclei per squared micrometers), the TUNEL-positive stained nuclei (per squared micrometers), and the rate of TUNEL-positive nuclei (per 10^5 nuclei).

Quantitative real-time PCR. Total RNA was isolated by acid-phenol extraction in the presence of chaotropic salts (TRIzol; Invitrogen, Carlsbad, CA) and subsequent isopropanol-ethanol precipitation as described previously (18, 27). Real-time RT-PCR of each sample was carried out with a TaqMan RNA PCR kit and ABI Prism 7500 Sequence Detection System (Applied Biosystems, Foster City, CA) according to the manufacturer's protocol. Expression of the housekeeping gene GAPDH was used for normalization. Bcl-2, Bcl-xL, Bax, and Bad assays were purchased as preoptimized kits from Applied Biosystems.

Immunohistochemical studies. Immunohistochemical studies were performed employing immunoperoxidase methods (18, 20). Hearts were fixed in Formalin, embedded in paraffin, and cut into 5-μm-thick cross sections. The sections were stained with antibodies against F4/80 (Novus Biological, Littleton, CO; dilution 1:50) for monocyte-derived macrophages, monocyte chemotactic protein (MCP)-1 (Hycult Biotech; Uden, The Netherlands; dilution 1:50), matrix metalloproteinase (MMP)-9 (Abcam, Cambridge, MA; dilution 1:100), and human CRP (Epitomics; Burlingame, CA; dilution 1:100). Because antibodies against neutrophils (Abcam; dilution 1:100) crossreacted with phagocytic macrophages, neutrophils were counted in the sections stained with hematoxylin and eosin by morphological assessment. For quantitative analysis, the number of positive cells was counted per field for five random fields and expressed as the number per squared millimeters.

Western blot analysis. LV samples were homogenized with lysis buffer containing 1% Triton X-100 and protease inhibitors. After centrifugation at 16,000 *g* for 30 min at 4°C, the supernatants were collected. Western blot analysis was performed as previously described (30). Equal quantities of proteins from LV samples were loaded on gels. Antibodies to MCP-1 (Abcam) and uncleaved and cleaved caspase-3 (Cell Signaling Technology, Danvers, MA) were used. After membranes were probed with primary antibodies, they were stripped of bound immunoglobulins and reprobed with anti-mouse GAPDH (Santa Cruz Biotechnology, Santa Cruz, CA) to correct for protein loading. The bands on the X-ray film were quantified by scanning densitometry with the ImageJ software and expressed as a percentage of the control.

Zymography. Gelatin zymography was performed to assess the activities of MMP-2 and MMP-9. Equal volumes of tissue extract from LV samples (10 μg of protein) were loaded on 10% SDS-polyacrylamide gels containing 1 mg/ml of gelatin (Novex Zymogram Gels; Invitrogen). The gels were incubated in renaturing buffer (2.5% Triton X-100) and then incubated in developing buffer at 37°C for 24 h (50 mM Tris·HCl, 10 mM $CaCl_2$). The gels were stained with 0.5% Coomassie Blue. Areas of protease activity appear as clear bands against a dark blue background where the protease has digested the gelatin substrate.

Serum MCP-1 measurement. Serum MCP-1 levels were measured by quantitative sandwich enzyme immunoassay technique using the Quantikine kit (R&D Systems) according to the manufacturer's instruction.

Table 1. *Morphometric data of control and CRP-Tg mice non-MI and post-MI*

	Non-MI		Post-MI		
	Control	CRP-Tg	Control	CRP-Tg	ANOVA
n	8	8	14	14	
BW, g	28.8 ± 2.3	28.0 ± 2.1	30.2 ± 3.1	29.4 ± 3.8	ns
LV + RV, mg	118 ± 13	112 ± 8	158 ± 15*	182 ± 14*†	$P < 0.0001$
(LV + RV)/BW, mg/g	4.1 ± 0.4	4.0 ± 0.4	5.3 ± 0.7*	6.3 ± 0.9*†	$P < 0.0001$
Lung, mg	160 ± 21	161 ± 12	174 ± 16	203 ± 31*†	$P = 0.0001$
Lung/BW, mg/g	5.6 ± 0.7	5.8 ± 0.5	5.8 ± 0.8	7.0 ± 1.4*†	$P = 0.003$
Liver, mg	1,285 ± 171	1,244 ± 153	1,199 ± 91	1,176 ± 153	ns
Liver/BW, mg/g	44.8 ± 5.6	44.5 ± 4.3	40.0 ± 3.8	40.2 ± 4.6	$P = 0.02$

Values are means ± SD; *n*, number of animals studied. CRP-Tg, transgenic mice with human C-reactive protein expression; MI, myocardial infarction; BW, body weight; LV, left ventricle; RV, right ventricle; ns, not significant. *$P < 0.05$, non-MI vs. post-MI; †$P < 0.05$, post-MI CRP-Tg vs. post-MI control (Bonferroni's test).

Statistical analysis. Results are presented as counts or means ± SD. Group comparisons were made using the Student's *t*-test (two tailed), the Mann-Whitney U test or the one-way ANOVA with Bonferroni's post hoc test for continuous data. Survival curves were computed using the Kaplan-Meier method and compared using the log rank test. The null hypothesis was rejected if $P < 0.05$. Analyses were performed using the GraphPad Prism (GraphPad software; San Diego, CA).

RESULTS

Characterization of CRP-Tg. There were no differences in phenotypic features including general appearance, body weight, and organ weights between control and CRP-Tg mice in the non-MI setting (Table 1). Systolic blood pressures measured by the tail-cuff method were similar in control and

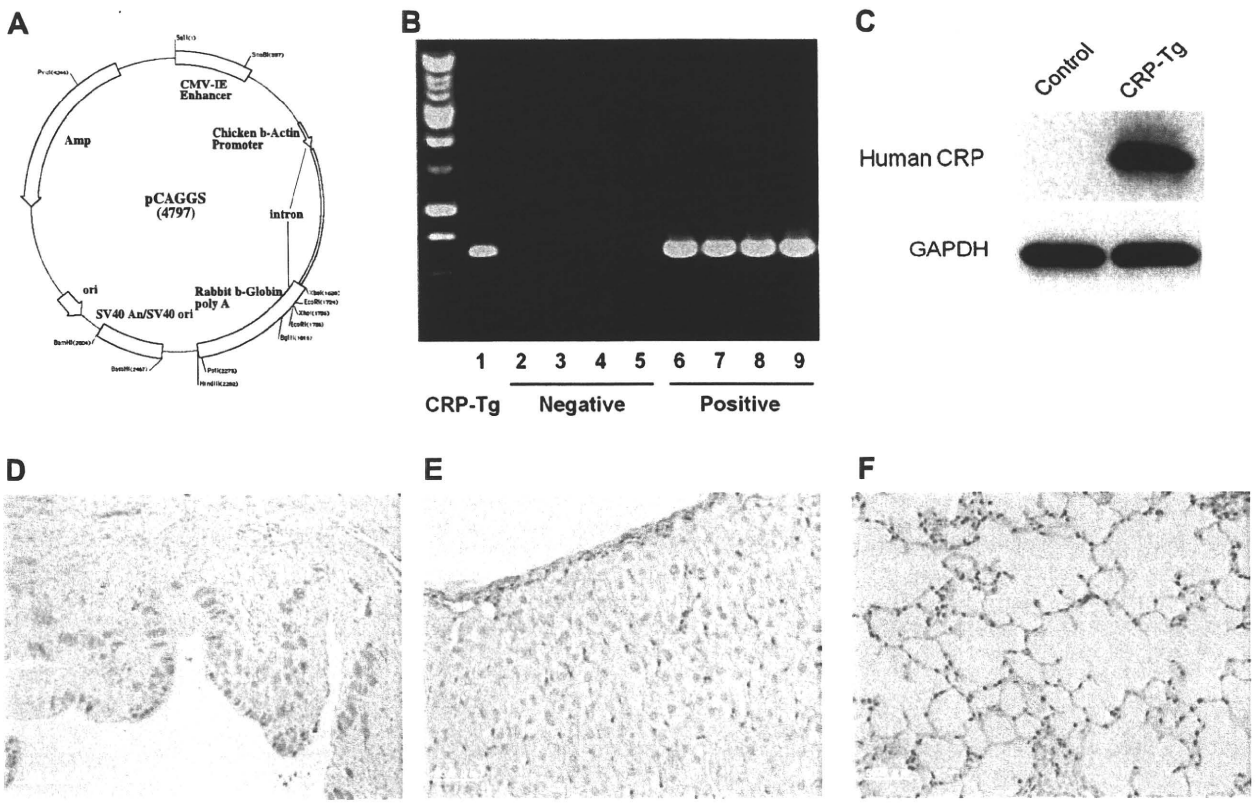

Fig. 1. Generation and characterization of transgenic mice with human C-reactive protein (CRP) expression (CRP-Tg) mice. *A*: human CRP cDNA was inserted into the unique *Eco*RI site between the CAG (modified chicken β-actin promoter with CMV-IE enhancer) promoter and 3′-flanking sequence of the rabbit β-globin gene of the pCAGGS expression vector. *B*: gene expression was confirmed by RT-PCR using genomic DNA extracted from clipped tails. *Lane 1* is the positive control. *Lanes 2-5* are samples negative for the CRP transgene, and *lanes 6-9* from positive samples. *C*: Western blotting of left ventricular (LV) homogenates showed marked protein expression of human CRP in LV samples from CRP-Tg mice but not in those from control mice. *D–F*: immunohistochemical studies confirmed local expression of human CRP (stained in brown) in sections from heart (*D*, 200×), liver (*E*, 400×), and lung (*F*, 400×).

CRP-Tg mice before MI (control, 106 ± 6 mmHg; CRP-Tg, 105 ± 9 mmHg, $n = 10$ for each group; $P = 0.77$). Heart rates were also similar in control and CRP-Tg mice (control, 574 ± 84 beats/min; CRP-Tg, 575 ± 56 beats/min, $n = 10$ for each group; $P = 0.96$). Serum CRP levels were 32 ± 7 mg/l in non-MI CRP-Tg mice ($n = 8$), whereas CRP was undetectable in serum from control mice. Histological examination in the hearts from CRP-Tg mice identified cardiac myocytes and endothelial cells as a main source of human CRP (Fig. 1*D*). No pathological abnormalities such as inflammation, hypertrophy, and fibrosis were seen in the hearts from non-MI CRP-Tg mice, which were indistinguishable from those from control mice. The count of neutrophils in the hearts was not different between control and CRP-Tg mice (control, 15 ± 6 cells/mm^2; CRP-Tg, 16 ± 6 cells/mm^2, $n = 6$ for each group; $P = 0.81$). The count of macrophages in the hearts was also comparable between the two groups (control, 4 ± 4 cells/mm^2; CRP-Tg, 5 ± 3 cells/mm^2, $n = 6$ for each group; $P = 0.68$).

Mortality and infarct size do not differ between control and CRP-Tg mice after MI. A total of 86 mice (45 controls and 41 CRP-Tg) underwent surgery for the survival study. Eleven mice (5 controls and 6 CRP-Tg) died of surgical complications: five mice (3 controls and 2 CRP-Tg) died before coronary ligation, three mice (2 controls and 1 CRP-Tg) died after coronary ligation but before extubation, and three mice (0 controls and 3 CRP-Tg) died immediately after extubation. The remaining 75 mice, consisting of 40 controls and 35 CRP-Tg mice, were included in the survival study. Kaplan-Meier analysis revealed that survival 5 wk after MI did not differ between the two groups (Fig. 2*A*). All animals had anterior wall MI at necropsy. LV rupture was found in six control mice and five CRP-Tg mice. Serum CRP levels were 43 ± 17 mg/l in the CRP-Tg mice that were euthanized 5 wk post-MI ($n = 14$).

We measured infarct sizes at 1 and 5 wk following MI using two approaches: *1*) the ratio of infarct area to total LV area in the LV samples that were cut and opened and *2*) the ratio of infarct lengths to total LV circumferences in the LV cross sections. Infarct size as assessed by either approach was comparable between the two groups (Fig. 2, *D* and *E*). Serum CRP levels were 51 ± 20 mg/l in the CRP-Tg mice that were euthanized 1 wk post-MI ($n = 10$). In addition, a separate group of animals were euthanized 24 h after MI to assess infarct size by TTC staining. Histological examination showed infarct size to be similar in the two groups ($P = 0.85$; Fig. 2, *C* and *F*). Infarct size was consistent with our previous data obtained using the same procedure (30). These results indicate that infarct size is not affected by human CRP expression in mice.

CRP-Tg mice have more prominent cardiac hypertrophy and fibrosis in the noninfarcted regions after MI than controls. As shown in Table 1, there was no group difference in body weight 5 wk after MI. The left and right ventricle weight and the left and right ventricle-to-body weight ratio were increased after MI, and these parameters were significantly higher in post-MI CRP-Tg mice than in post-MI controls. The lung weight and the lung-to-body weight ratio were higher in post-MI CRP-Tg mice than in post-MI controls. These data suggest that cardiac hypertrophy and lung congestion associated with MI are more pronounced in CRP-Tg mice.

Histological evaluation revealed the cross-sectional area of cardiac myocytes in the noninfarcted intraventricular septum was increased 5 wk after MI, and the increase in cardiomyo-

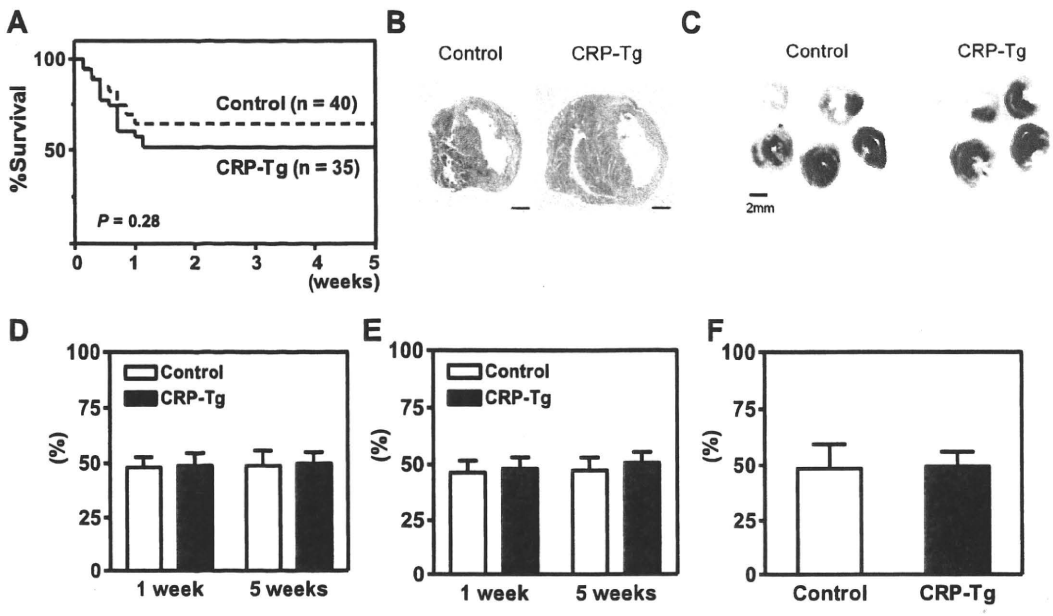

Fig. 2. *A*: seventy-five mice (40 controls and 35 CRP-Tg mice) that recovered from surgery were subjected to the survival study. Kaplan-Meier curve analysis demonstrated that mortality at 5 wk did not differ between the 2 groups (log rank, $P = 0.28$). *B*: transverse sections of LV at the midventricular level from a control mouse and a CRP-Tg mouse 1 wk after myocardial infarction (MI); Masson's trichrome. *C*: representative pictures of sliced LV cross sections obtained from a control mouse and a CRP-Tg mouse 24 h after MI. Necrotic tissues (white) are distinct from viable tissues (red); 1% triphenyltetrazolium chloride (TTC). *D*: there was no group difference in infarct size 1 and 5 wk after MI as assessed by the ratio of infarct area to total LV area in LV samples. *E*: no group difference in infarct size was found as assessed by the ratio of infarct lengths to total LV circumferences in LV cross sections. *F*: histological examination by TTC staining showed infarct size to be similar in the 2 groups 24 h after MI.

Table 2. *Echocardiographic data of control and CRP-Tg mice before and after MI*

	Pre-MI		Post-MI		
	Control	CRP-Tg	Control	CRP-Tg	ANOVA
n	17	14	17	14	
HR, beats/min	485 ± 56	454 ± 43	492 ± 50	475 ± 53	ns
LVEDD, mm	3.3 ± 0.3	3.2 ± 0.3	5.2 ± 0.5*	5.8 ± 0.4*†	$P < 0.0001$
LVESD, mm	1.7 ± 0.3	1.6 ± 0.3	4.6 ± 0.6*	5.2 ± 0.4*†	$P < 0.0001$
AWth, mm	0.69 ± 0.04	0.69 ± 0.04	0.42 ± 0.07*	0.40 ± 0.05*	$P < 0.0001$
PWth, mm	0.68 ± 0.04	0.68 ± 0.05	0.59 ± 0.08*	0.55 ± 0.08*	$P < 0.0001$
LVEF, %	67 ± 6	67 ± 8	19 ± 5*	13 ± 5*†	$P < 0.0001$

Values are means ± SD; *n*, number of animals studied. HR, heart rate; LVEDD, left ventricular end-diastolic diameter; LVESD, left ventricular end-systolic diameter; AWth, anterior wall thickness; PWth, posterior wall thickness; LVEF, left ventricular ejection fraction. *$P < 0.05$, post-MI vs. pre-MI; †$P < 0.05$, post-MI CRP-Tg vs. post-MI control (Bonferroni's test).

cyte cross-sectional area was greater in CRP-Tg mice than in controls (non-MI control, 270 ± 12 μm^2; non-MI CRP-Tg, 268 ± 16 μm^2; MI control, 389 ± 25 μm^2; MI CRP-Tg, 474 ± 62 μm^2, $n = 6$ for each group; $P < 0.05$ from one-way ANOVA with Bonferroni's test). Staining with Masson's trichrome showed cardiac fibrosis in the noninfarcted intraventricular septum to be enhanced in CRP-Tg mice than in controls 5 wk after MI (control, 0.17 ± 0.05%; CRP-Tg, 0.29 ± 0.07%, $n = 6$ for each group; $P = 0.01$), whereas there was no group difference in percent area of fibrosis in the infarct region (control, 84.8 ± 2.4%; CRP-Tg, 85.6 ± 4.3%, $n = 6$ for each group; $P = 0.68$).

CRP-Tg mice have more LV dilation and worse LV function after MI than controls. Table 2 shows echocardiographic findings before MI and 5 wk after MI. Before MI, there were no differences in heart rate, LV dimensions, wall thickness, or LV function between CRP-Tg and control mice. Five weeks after MI, heart rates did not change. Both anterior and posterior wall thickness decreased to the same extent in both groups. However, LV end-diastolic and end-systolic diameters were larger in CRP-Tg mice, indicating increased chamber dilation. In addition, CRP-Tg mice had lower LV EFs than control mice. To investigate the effects of increased CRP expression on LV remodeling and function at an earlier time point, a different group of animals underwent echocardiography 1 wk after MI. When compared with that of control mice, CRP-Tg mice had larger LV end-diastolic diameter (control, 4.4 ± 0.4 mm, $n = 11$; CRP-Tg, 5.3 ± 0.4 mm, $n = 10$; $P < 0.0001$) and LV end-systolic diameter (control, 3.7 ± 0.5 mm, $n = 11$; CRP-Tg, 4.6 ± 0.4 mm, $n = 10$; $P = 0.0002$) and lower LV EFs (control, 21 ± 5%, $n = 11$; CRP-Tg, 15 ± 4%, $n = 10$; $P = 0.009$). Therefore, the differences in LV size and function between the two groups were already apparent 1 wk after MI. These data suggest that increased CRP expression is associated with more LV dilation and worse LV function after MI.

Hemodynamic measurements were conducted 5 wk after MI. Heart rate, aortic pressure, and LV systolic and end-diastolic pressures did not differ between the CRP-Tg and control groups (Table 3). LV +dP/d*t* was lower in the CRP-Tg group than in the control group ($P = 0.006$). LV −dP/d*t* was also reduced in CRP-Tg mice ($P = 0.002$). These data indicate that increased CRP expression adversely affects LV contractility and relaxation after MI.

Increased apoptosis in the border zones of infarcted hearts from CRP-Tg mice. There were very few TUNEL-positive nuclei in LV sections from uninfarcted mice, and no group difference in the number of TUNEL-positive nuclei was found (control, 12 ± 5 nuclei per 10^5 cells; CRP-Tg, 14 ± 6 nuclei per 10^5 cells, $n = 6$ for each group; $P = 0.46$). This finding indicates that myocardial apoptosis is not induced by human CRP expression in mice under physiological conditions. At 1 wk post-MI, TUNEL-positive nuclei were observed more frequently in the border and infarct zones than in the remote zones in the both groups, which is consistent with our previous findings (30). The rate of myocardial apoptosis in the border zone was higher in the CRP-Tg group than in the control group 1 wk after MI induction (control, 596 ± 275 nuclei per 10^5 cells; CRP-Tg, 1,434 ± 789 nuclei per 10^5 cells, $n = 6$ for each group; $P = 0.03$), whereas the apoptotic rates in the remote and the infarct zones were similar in the two groups (remote: control, 50 ± 12 nuclei per 10^5 cells, and CRP-Tg, 63 ± 24 nuclei per 10^5 cells, $n = 6$ for each group, $P = 0.57$; and infarct: control, 723 ± 314 nuclei per 10^5 cells, and CRP-Tg, 781 ± 435 nuclei per 10^5 cells, $n = 6$ for each group, $P = 0.81$; Fig. 3, *A–C*). We also assessed expression of apoptosis-related genes such as Bcl-2, Bcl-xL, Bax, and Bad in homogenates from the remote, the border, and the infarct zones by real-time RT-PCR ($n = 6$ for each group). Bcl-2 expression in the border zone was decreased by 41% in the CRP-Tg group compared with the control group ($P < 0.05$; Fig. 3*D*). Bcl-2 expression was lower in the infarct zone than in the remote zone, but no group difference in Bcl-2 levels was found in the infarct zone. In contrast, Bax expression in the border zone was increased by 56% in the CRP-Tg group ($P < 0.05$; Fig. 3*E*). Bax expression

Table 3. *Hemodynamic data of control and CRP-Tg mice after MI*

	Control	CRP-Tg
n	10	9
HR, beats/min	402 ± 73	373 ± 75
SBP, mmHg	81 ± 10	76 ± 8
DBP, mmHg	55 ± 9	49 ± 8
LVSP, mmHg	82 ± 11	78 ± 7
LVEDP, mmHg	11 ± 4	13 ± 3
LV +dP/d*t*, mmHg/s	3,788 ± 656	2,974 ± 509*
LV −dP/d*t*, mmHg/s	−2,890 ± 480	−2,230 ± 143*

Values are means ± SD; *n*, number of animals studied. SBP, systolic blood pressure; DBP, diastolic blood pressure; LVSP, left ventricular systolic pressure; LVEDP, left ventricular end-diastolic pressure; LV +dP/d*t*, left ventricular positive change in pressure over time; LV −dP/d*t*, left ventricular negative change in pressure over time. *$P < 0.01$, CRP-Tg vs. control (Student's unpaired *t*-test, 2-tails).

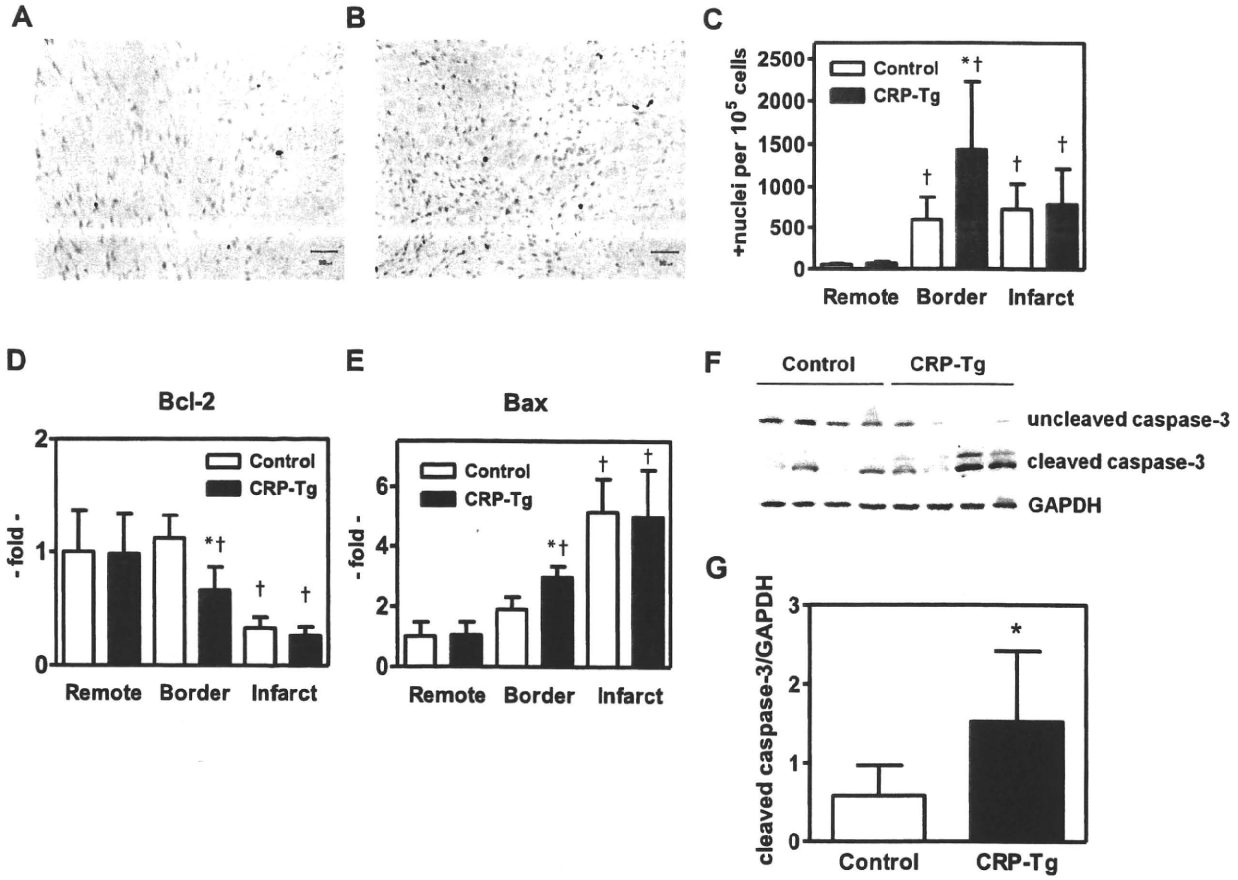

Fig. 3. *A* and *B*: photomicrographs showing blue-stained nuclei (apoptotic) in section of left ventricle from the border zone of a control mouse (*A*) and a CRP-Tg mouse (*B*); TUNEL staining, 400×. *C*: TUNEL-positive nuclei were more frequently observed in the border and the infarct zones than in the remote zones. Apoptotic rate in the border zone was higher in CRP-Tg mice than in control mice 1 wk after MI. *D*: real time RT-PCR showed Bcl-2 expression in the border zone to be lower in CRP-Tg mice than in control mice. Bcl-2 expression was lower in the infarct zone than in the remote zone, but no group difference in Bcl-2 levels was found in the infarct zone. *E*: Bax expression in the border zone was higher in CRP-Tg mice than in control mice. Bax expression was higher in the infarct zone than in the remote zone, but no group difference in Bax levels was found in the infarct zone. Expression of the housekeeping gene GAPDH was used for normalization. *F*: Western blotting of border zone samples for uncleaved caspase-3 and cleaved (active) caspase-3. Increased cleaved caspase-3 content was found in border zone samples from CRP-Tg mice compared with control mice; total caspase-3 was unchanged. *G*: quantification of immunoblotting showed that cleaved caspase-3 expression was higher in border zone samples from CRP-Tg mice compared with control mice. Values are normalized against the corresponding GAPDH levels. Data are means ± SD; $n = 6$ for both groups. *$P < 0.05$, border CRP-Tg vs. border control; †$P < 0.05$, border vs. remote; infarct vs. remote (nonparametric test).

was higher in the infarct zone than in the remote zone, but no group difference in Bax levels was found in the infarct zone. There were no significant group differences in border zone Bcl-xL expression (control, 1.7 ± 0.8 arbitrary unit; CRP-Tg, 1.0 ± 0.4 arbitrary unit; $P = 0.05$) and Bad expression (control, 2.7 ± 0.7 arbitrary unit; CRP-Tg, 4.5 ± 2.1 arbitrary unit; $P = 0.11$). These data suggest that alterations in Bcl-2 and Bax expression are associated with promotion of apoptosis in the border zones of infarcted hearts from CRP-Tg mice. In addition, Western blot analysis showed protein content of cleaved (active form) caspase-3 to be increased in the border zone samples from CRP-Tg mice compared with those from control mice ($P = 0.02$; Fig. 3, *F* and *G*); the sum of uncleaved and cleaved caspase-3 levels was unchanged.

Increased macrophage infiltration, MCP-1 expression, and MMP-9 activity in the border zones of infarcted hearts from CRP-Tg mice. In histological studies, apparent inflammation was seen in the border and the infarct areas but not in the remote region of 1-wk old infarcted hearts. Immunohistochemical studies revealed infiltrating macrophages, as demonstrated by staining with anti-F4/80 antibodies, were predominantly found in the border and the infarct zones. More abundant macrophages (brown stained) were observed in the border zones of infarcted hearts from CRP-Tg mice compared with those from controls ($P = 0.01$; Fig. 4, *A–C*), although the number of macrophages in the infarct zone was comparable between the two groups ($P = 0.30$). The infiltration of neutrophils in the border and the infarct zones, which was a relatively low percentage of infiltrating inflammatory cells at 1 wk post-MI, was similar in the two groups (border: control, 66 ± 18 cells/mm^2, and CRP-Tg, 65 ± 11 cells/mm^2, $P = 0.85$; and infarct: control, 64 ± 10 cells/mm^2, and CRP-Tg 73 ± 10 cells/mm^2, $n = 6$ for each group, $P = 0.43$).

Increased MCP-1 expression in the border zones of infarcted hearts from CRP-Tg mice. Immunohistochemical studies identified macrophages infiltrating in the border and the

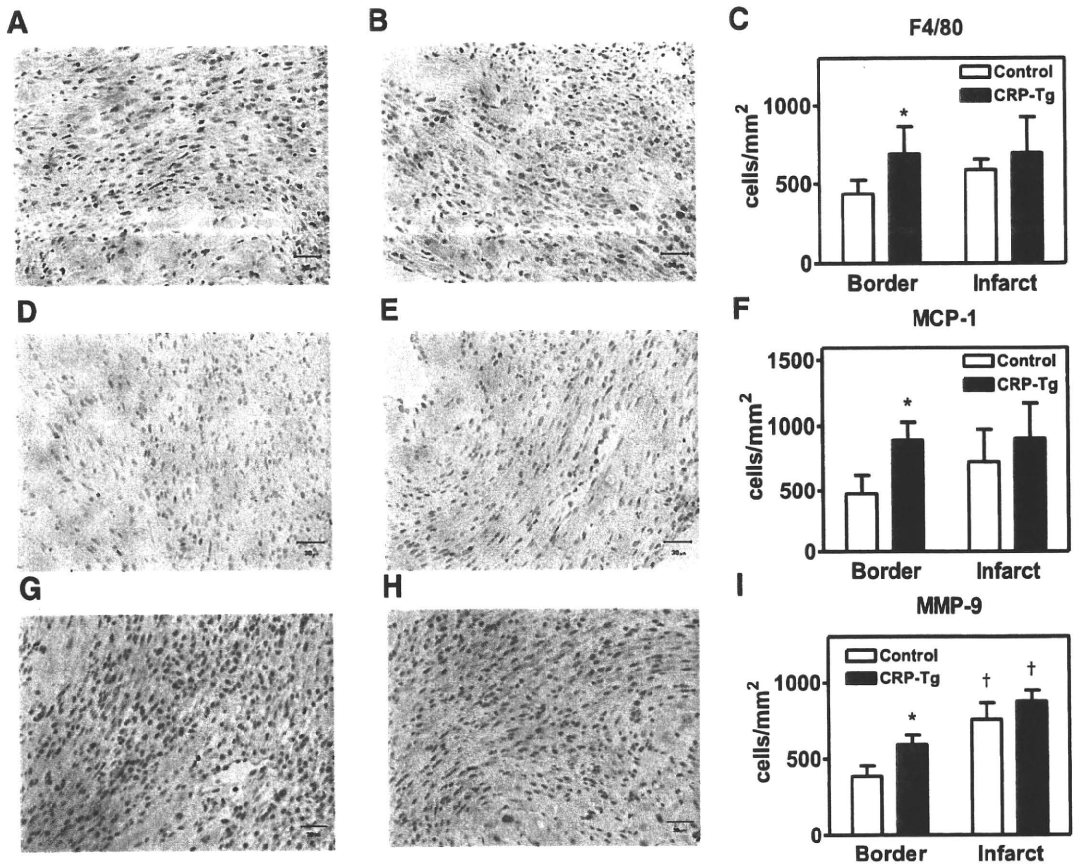

Fig. 4. Immunohistochemical studies stained with antibodies against F4/80 (macrophages), monocyte chemotactic protein (MCP)-1, and matrix metalloproteinase (MMP)-9. *A* and *B*: representative photomicrographs showing brown-stained F4/80 positive cells in a section of the border zone from a control mouse (*A*) and a CRP-Tg mouse (*B*), 400×. *C*: infiltration of F4/80 positive cells was more abundant in the border zones of CRP-Tg mice than in those of control mice 1 wk after MI. *D* and *E*: representative photomicrographs showing brown-stained MCP-1 positive cells in a section of the border zone from a control mouse (*D*) and a CRP-Tg mouse (*E*), 400×. *F*: MCP-1 expression was predominantly found in infiltrating macrophages in the border and infarct zones. More MCP-1 positive cells were seen in the border zones of infarcted hearts from CRP-Tg mice than those from control mice. *G* and *H*: representative photomicrographs showing brown-stained MMP-9 positive cells in a section of the border zone from a control mouse (*G*) and a CRP-Tg mouse (*H*), 400×. *I*: MMP-9 expression was predominantly found in leucocytes and macrophages infiltrating in the border and infarct zones. MMP-9 positive cells were more frequently observed in the infarct zone than in the border zones. More MMP-9 positive cells were seen in the border zones of infarcted hearts from CRP-Tg mice than those from control mice. Data are means ± SD; $n = 6$ for each group. *$P < 0.05$, border CRP-Tg vs. border control; †$P < 0.05$, infarct vs. border (Bonferroni's test).

infarct zones as a main source of MCP-1 (brown stained; Fig. 4, *D* and *E*). More MCP-1 positive cells were seen in the border zones of infarcted hearts from CRP-Tg mice than those from control mice, although there was no group difference in the number of MCP-1 positive cells in the infarct zone (Fig. 4*F*). Western blot analysis also showed MCP-1 protein expression to be increased by 1.5-fold in the border zones, but not in the infarct zone, of infarcted hearts from CRP-Tg mice compared with those from control mice ($P < 0.05$; Fig. 5). MCP-1 expression in remote zone samples was too weak to be detected as clear bands by immunoblotting (data not shown). Serum MCP-1 levels at 1 wk following MI were similar in the two groups (control, 56 ± 24 pg/ml; CRP-Tg, 62 ± 23 pg/ml, $n = 6$ for each group; $P = 0.64$).

Increased MMP-9 activity in the infarct and the border zones of infarcted hearts from CRP-Tg mice. Immunohistochemical studies revealed that MMP-9 expression (brown stained) was predominantly found in leucocytes and macrophages infiltrating in the border and the infarct zones (Fig. 4, *G* and *H*). MMP-9 expression was more frequently observed in the infarct zone than in the border zones. In addition, more MMP-9 positive cells were found in the border zones of infarcted hearts from CRP-Tg mice than those from control mice (Fig. 4*I*). Gelatin zymography showed MMP-9 activity to be higher in border and infarct zones samples from CRP-Tg mice than in those from control mice at 1 wk following MI (Fig. 6, *A–C*). Although MMP-2 activity was enhanced in the border and the infarct zones of infarcted hearts, no group difference in MMP-2 activity was found in either region (Fig. 6*D*).

DISCUSSION

We found that CRP-Tg mice showed greater LV dilation and had poorer LV function with more prominent cardiomyocyte hypertrophy and fibrosis in the viable intraventricular septum after MI than control mice, although survival and infarct size were similar in the two groups. This adverse effect of CRP on LV remodeling was already apparent 1 wk after MI, suggesting a pathogenic role of CRP in the early phase of the post-MI remodeling process. The current study also showed higher

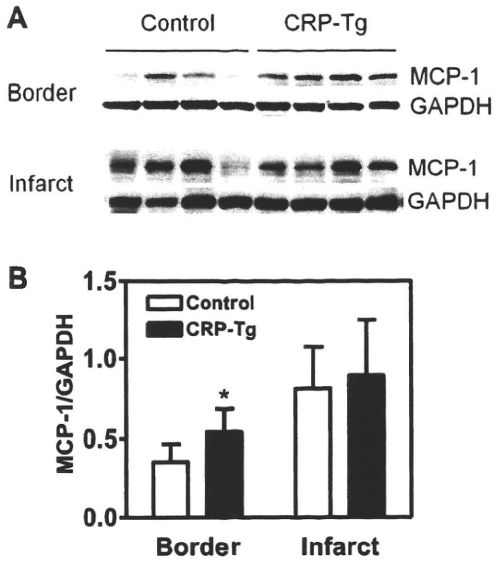

Fig. 5. Western blotting for MCP-1. *A*: increased MCP-1 expression was found in border zone samples from CRP-Tg mice than those from control mice. *B*: quantification of immunoblotting results showed the MCP-1 content to be 1.5-fold higher in border zone samples from CRP-Tg mice than in those from control mice. No group difference was found in infarct zone samples. Values are normalized against the corresponding GAPDH levels. Data are means ± SD; $n = 6$ for each group. *$P < 0.05$, CRP-Tg vs. control (nonparametric test).

apoptotic rates, more macrophage infiltration, and increased MCP-1 expression and MMP-9 activity in the border zones of infarcted hearts from CRP-Tg mice.

CRP is an acute-phase reactant, which responds to various pathological stimuli including infection, inflammation, tissue damage, and neoplasm. Recent experimental studies indicate that CRP per se has multiple biological activities that may be involved in the pathophysiology of various cardiovascular diseases. For instance, CRP induces expressions of adhesion molecules and chemokines such as MCP-1 in in vitro studies (10). CRP reportedly induces apoptosis in human vascular smooth muscle cells as well as rat cardiac myocytes (6, 33). CRP was also reported to attenuate survival, differentiation, and the functions of endothelial progenitor cells (32). CRP-Tg mice that constitutively produce human CRP provide a useful model for studying the biological activities of human CRP in vivo. Some investigators using a crossbreeding method have reported that human CRP expression accelerates the progression of atherosclerosis in apoE-deficient mice (22, 26), although conflicting data have been presented by other laboratories (12, 14, 31).

In acute MI, CRP peaks at 2 to 3 days after the onset, and the peak level is a strong predictor of adverse clinical outcomes (2, 3, 29). Although the pathogenic importance of CRP remains undetermined in the acute MI setting, CRP colocalizes with activated complement in human infarcted tissues (15). Griselli et al. (9) reported that injection of human CRP after coronary artery occlusion increases infarct size in rats. In the present study, however, increased CRP expression did not affect infarct size in our transgenic mouse model. This difference may be explained by the different species (mouse vs. rat) used, the different experimental conditions (transgene expression vs. protein injection), and the extent of infarct size. The average infarct size was ~50% in our study, whereas it was 17% for the vehicle-treated group and 25% for the CRP-treated group in their study (9). It is noteworthy that, in our study, increased CRP expression was associated with more LV dilation and worse LV function after MI without altering infarct size. To our knowledge, no study has shown direct in vivo effects of CRP on the development of adverse LV remodeling after MI. We therefore asked how increased CRP expression could modulate the post-MI inflammatory response and healing process as well as apoptosis, which might be responsible for deterioration of cardiac remodeling after MI in our CRP-Tg mice.

The post-MI inflammatory response plays a critical role in the pathophysiology of infarct expansion and LV remodeling (8). We previously reported post-MI peripheral monocytosis to be associated with LV dysfunction and LV aneurysm (17) and that granulocyte-macrophage colony-stimulating factor induction in a rat MI model resulted in exaggerated LV remodeling

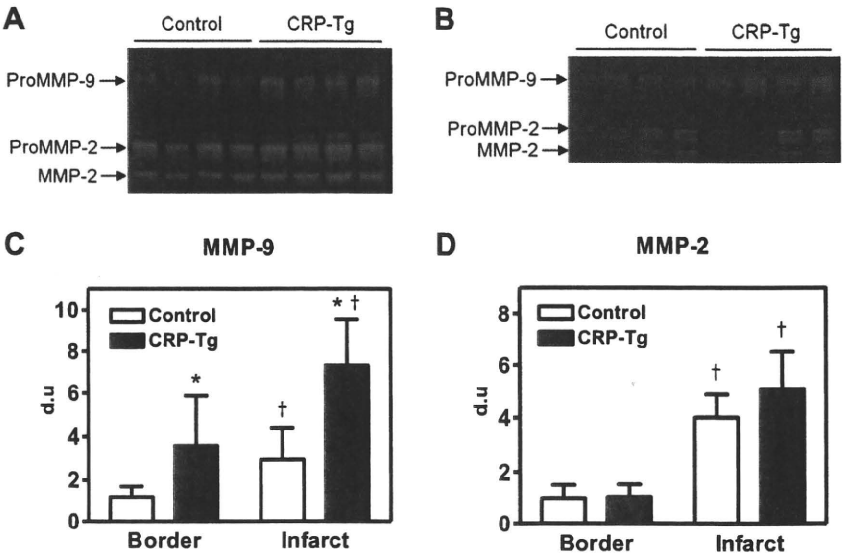

Fig. 6. *A* and *B*: gelatin zymography for MMP activities in infarct zone samples (*A*) and border zone samples (*B*). *C*: MMP-9 activity in the border and the infarct zones was increased in CRP-Tg mice 1 wk after MI. *D*: although MMP-2 activity was enhanced in the border and the infarct zones of infarcted hearts, no group difference in MMP-2 activity was found in either region. Data are means ± SD; $n = 6$ for each group. *$P < 0.05$, border CRP-Tg vs. border control; †$P < 0.05$, infarct vs. border (nonparametric test). du, Densitometric unit.